Engineering Structures 292 (2023) 116536

Contents lists available at ScienceDirect

Engineering Structures

journal homepage: www.elsevier.com/locate/engstruct

Bond behavior of FRP-concrete wet-bonding interface under lateral confinement

Hongwei Lin [a,b,c], Huixin Zeng [a], Peng Feng [c,*], Cheng Jiang [d], Yuqing Zhang [e]

[a] School of Civil Engineering, Beijing Jiaotong University, Haidian District, Beijing 100044, China
[b] Key Laboratory of Concrete and Prestressed Concrete Structures of Ministry of Education, Southeast University, Nanjing 210096, China
[c] Department of Civil Engineering, Tsinghua University, Beijing 100084, China
[d] Centre for Infrastructure Engineering, Western Sydney University, Penrith, NSW 2751, Australia
[e] Zhongfu Carbon Fiber Core Cable Technology Co., Ltd, Lianyun Gang 222000, China

ARTICLE INFO

Keywords:
Fiber reinforced polymer (FRP)
Concrete
Wet-bonding
Interface
Bond-slip
Confinement

ABSTRACT

Wet-bonding is a technique of connecting fiber reinforced polymer (FRP) profile and cast-in-place concrete, which is characterized by the simultaneous hardening of concrete and adhesive. The mechanical properties of wet-bonding interface have been investigated by researchers, but none of them considers the influence of lateral confinement which is commonly present in structures. The insufficient knowledge on wet-bonding consequently hinders its application in FRP-concrete hybrid structures. To this end, this paper investigates the bond properties of wet-bonding interface in confined concrete through pullout and pushout tests. Test results indicate that the interfacial behavior of wet-bonding interface can be divided into three stages. In the first stage, the interfacial resistance comes from the chemical bond of adhesive, and the lateral confinement is hardly activated. This stage comes to an end when the interface between adhesive and concrete fails. In the second and third stage, the interfacial resistance is mainly contributed by the friction between fractured surfaces of adhesive and concrete. The relative movement of fractured surfaces which are microscopically rough induces vertical movement and then activates the lateral confinement, resulting in lateral pressure and tangential friction. The significant friction behavior further damages the FRP-adhesive interface, leading to the final delamination of adhesive from the FRP plate. Based on the above force-transfer mechanism, a bond stress-slip model depending on the lateral pressure is developed. This interfacial model is implemented into Abaqus and its effectiveness is verified by comparing with test results.

1. Introduction

Fiber reinforced polymer (FRP) as a composite material made of fiber and resin matrix has been increasingly used in civil engineering since 1980s [1,2]. With the advantages of lightweight, corrosion-resistance, high strength, and ease of fabrication, FRP provides structural engineers more choices in designing durable and lightweight structures or strengthening/retrofitting deficient structures. Among the applications of FRP, the hybrid utilization of concrete and FRP is promising, which can maximize the advantages of both materials [3–5]. Extensive studies can be found in the literature regarding FRP-concrete hybrid structures, and various composite members have been developed by researchers worldwide [6], including composite beams [7–11], composite slabs [12], composite columns [13–15], composite shear walls [16], etc. The mechanical properties of composite members are highly dependent on the interfacial behavior between FRP and concrete. Only with adequate interfacial resistance, can FRP-concrete hybrid structures work favorably [17]. Currently, the existing methods for connecting FRP and concrete include dry-bonding, wet-bonding, sand-coating, bolt connection, perforation, shear key, etc. Among these methods, wet-bonding technique has been a research focus due to its convenience in application.

Different with the traditional dry-bonding technique, which deals with the bond between existing concrete structure and FRP plates or sheets in the domain of structure strengthening, wet-bonding is a technique for connecting FRP plates and cast-in-place concrete. In the wet-bonding technique, the epoxy is firstly spread on the prefabricated FRP plate, and then wet concrete is poured on the adhesive-coated plate. The fresh concrete and adhesive cure simultaneously. The feasibility of

* Corresponding author.
E-mail address: fengpeng@tsinghua.edu.cn (P. Feng).

https://doi.org/10.1016/j.engstruct.2023.116536

Available online 11 July 2023

Nomenclature

B	empirical parameter	s_{cm}	corresponding slip of τ_{cm}
b_f	width of FRP plate	$s_{\delta max}$	corresponding slip of δ_{max}
E_f	elastic modulus of FRP plate	$s_{\mu max}$	corresponding slip of μ_{max}
f_c	compressive strength of concrete	t_a	thickness of adhesive layer
f_t	tensile strength of concrete	t_f	thickness of FRP plate
G_a	shear modulus of adhesive layer	s_{max}	corresponding slip of τ_{max}
G_f	interfacial fracture energy	α	empirical coefficient
K_{spring}	constant stiffness of springs	β_w	width ratio factor
K_{exp}	Lateral stiffness	δ	interfacial dilatation
k_δ	empirical parameter	δ_{max}	maximum dilatation
L	bond length	σ_{ip}	interfacial pressure
l_{coh}	length of cohesive element	μ_{max}	maximum friction coefficient
L_e	effective bond length	μ	friction coefficient
P	pushout or pullout load	τ	bond stress
P_u	peak load	τ_{cm}	maximum bond stress in stage I
s	relative slip	τ_c	adhesion component
		τ_f	friction component
		τ_{max}	ultimate bond stress

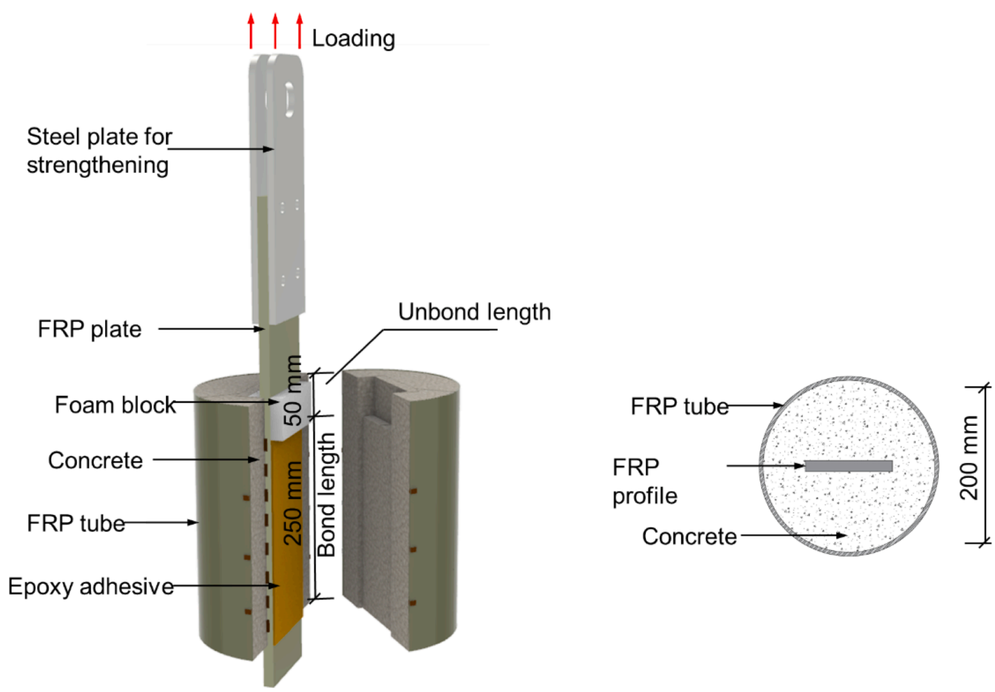

Fig. 1. Schematic illustration of the long-bond length specimen.

connecting fresh concrete and FRP plate via wet-bonding has been confirmed by a number of studies [18,19]. Some researchers even concluded that wet-bonding technique was the most appropriate method of connecting fresh concrete with FRP profile [20,21]. Specific study on the mechanical performance has been conducted by Shao [22], who found that the wet-bonding interface shared a similar interfacial behavior with dry-bonding. They further investigated the mechanical behavior of wet-bonding interface exposed to low temperature, freeze–thaw cycles and wet-dry cycles, and found that the wet-bonding interface had a thicker and more porous adhesive layer than dry-bonding interface [23]. Due to the moisture in fresh concrete, the epoxy of wet-bonding interface was inadequately cured. Consequently, the load capacity of wet-bonding interface was 11% lower than dry-bonding interface. However, wet-bonding interface showed better resistance to freeze–thaw cycles and wet-dry cycles. There are some other researchers who conducted tests on wet-bonding interface based on single shear tests or double shear tests or pushout tests [24–26], and the involved variables included setting time of adhesive, concrete age, type of adhesive, thickness of adhesive, etc. All tests indicate that the wet-bonding interface fails at the interface between adhesive and concrete with little mortar attaching to the FRP plate, which is different with dry-bonding characterized by concrete failure neighboring the interface. According to Zhang et al. [25,27], the shear bond strength and interfacial fracture energy of wet-bonding interface are 54%~68% and 30%~45% of those of dry-bonding interface. Based on well-known bond stress-slip models for dry-bonding interface, including model by Dai et al. [28] and model by Lu et al. [29–31], Wang et al. [24,32] and Zhang et al. [25,26] developed empirical models for wet-bonding interface. The wet-bonding interface of FRP profile and concrete shares similarities with the wet-bonding interface of wood and concrete. Yan et al. [33,34]

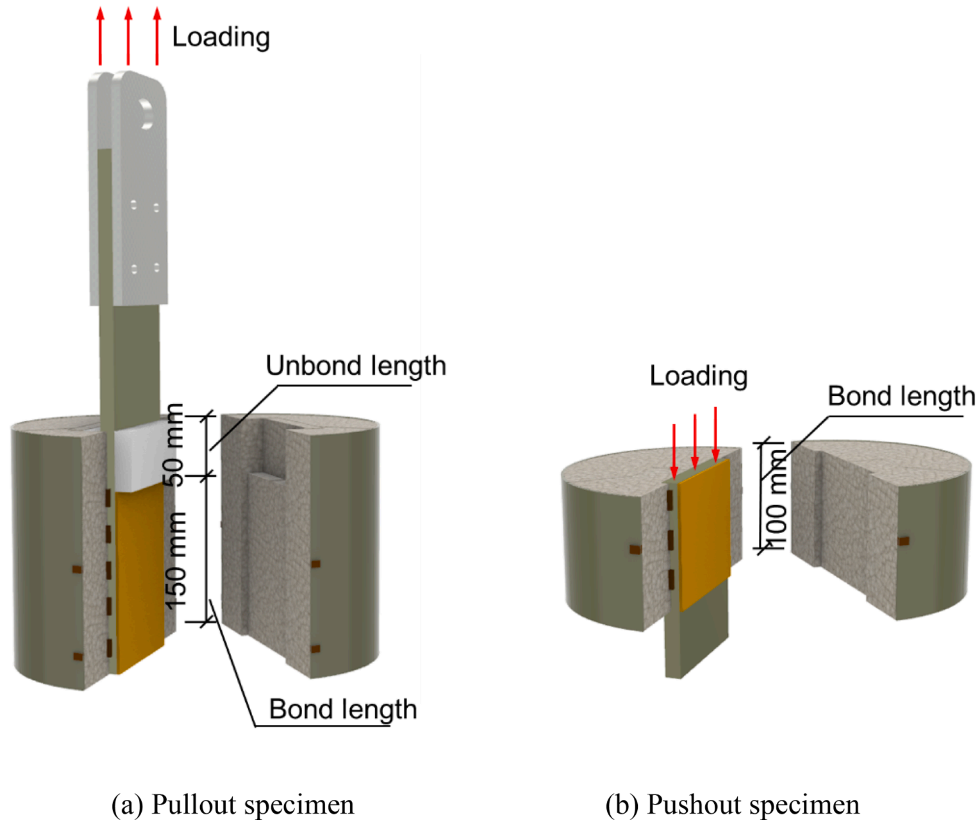

Fig. 2. Schematic illustration of the short-bond length specimen.

Table 1
Details of the tested specimens.

Designation	Height (mm)	Bond length (mm)	Unbond length (mm)	Loading method
C-W-1	300	250	50	Pullout loading
C-W-2	300	250	50	Pullout loading
C-W-3	300	250	50	Pullout loading
C-W-1-PL	200	150	50	Pullout loading
C-W-1-PS	100	100	0	Pushout loading
C-W-3-PL	200	150	50	Pullout loading
C-W-3-PS	100	100	0	Pushout loading

C-W-1/2/3 are long bond length specimens; C-W-1-PL/PS and C-W-3-PL/PS are short bond length specimens; PL means pullout loading, and PS means pushout loading.

Table 2
Concrete mixture proportions (kg/m^3).

Water	Cement	Fine aggregates	Coarse aggregates	Water reducing admixture
204	408	583	962	1.2

investigated the mechanical properties of the wet-bonding interface of wood and concrete based on double-shear tests, and found that the failure mode of the wet-bonding interface of concrete and wood is quite like that of the wet-bonding interface of concrete and FRP, i.e., failure occurs at the interface between wood and concrete. They further pointed out that the bond capacity of wet-bonding joint was close to that of dry-bonding joint when epoxy was used, while wet-bonding interface showed a smaller interfacial capacity when two-component polyurethane adhesive was applied.

A summary of the above studies reveals that a general knowledge regarding the bond properties of wet-bonding interface has been formulated, and empirical bond stress-slip relationship models have been proposed. However, a major drawback of these studies is that the influence of lateral confinement on the interfacial behavior of wet-bonding interface is hardly understood. The FRP-concrete interface is commonly subjected to lateral confinement in various forms. For instance, when FRP profile is embedded in concrete confined by stirrups [35] or steel tube [36] or FRP tube [37], lateral pressure will be developed at the FRP-concrete interface. Some studies have demonstrated that the lateral confinement can significantly change the interfacial behavior. Due to the normal pressure generated from the lateral confinement, significant friction will take place at the interface after initial debonding, resulting in a ductile interfacial behavior. This phenomenon has been documented in Biscaia et al. [38], Lee and Lopez [39,40], and Wu and Liu [41], in which bond stress-slip models for dry-bonding interface under specific lateral confinements were developed. Considering the shear-dilation effects, the first author of this paper proposed a pressure-dependent model for sand-coated FRP-concrete interface [3], which is applicable for different confinement conditions. Unfortunately, none of the studies discuss the influence of lateral confinement on the wet-bonding interface, which has limited the application of wet-bonding technique in FRP-concrete hybrid structures.

To fill the research gap, this paper investigates the bond properties of wet-bonding interface under lateral confinement based on pullout and pushout tests. The force-transfer mechanism of the wet-bonding interface is thoroughly analyzed and a bond stress-slip model with shear-dilation effects is proposed.

Table 3
Mechanical properties of the GFRP plates.

Thickness	Longitudinal direction					Transverse direction	
	Strength (MPa)			Young's modulus (GPa)		Compressive	
	Tensile	Compressive	In-plane shear	Tensile	Compressive	Strength (MPa)	Young's modulus (GPa)
12.7 mm	531	377	32.3	33.2	24.0	108.3	11.2

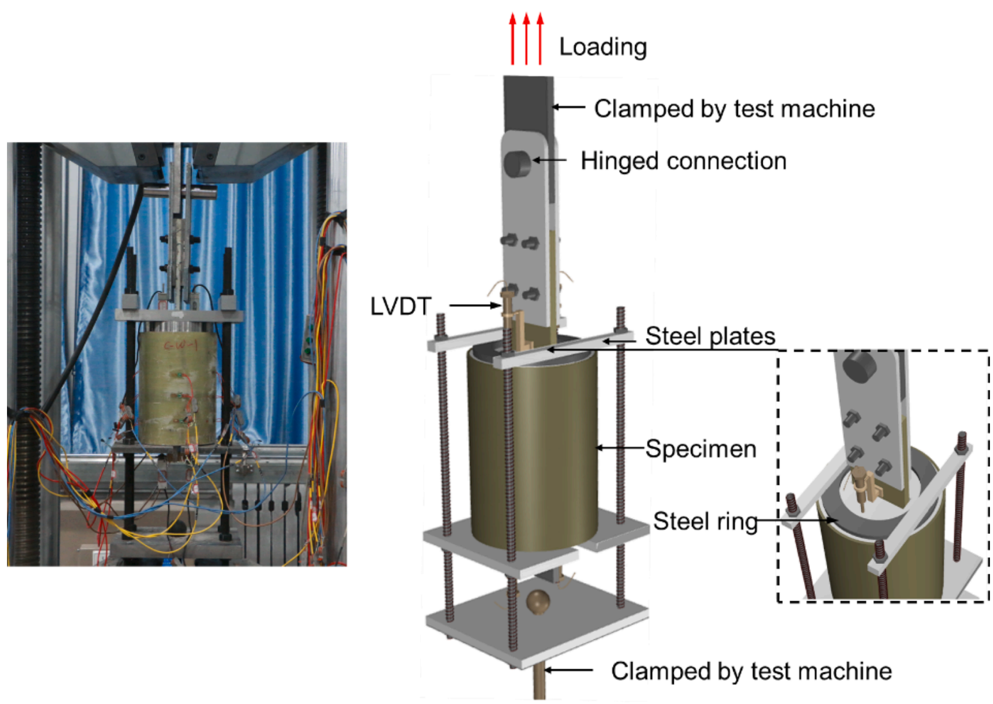

(a) Pullout tests

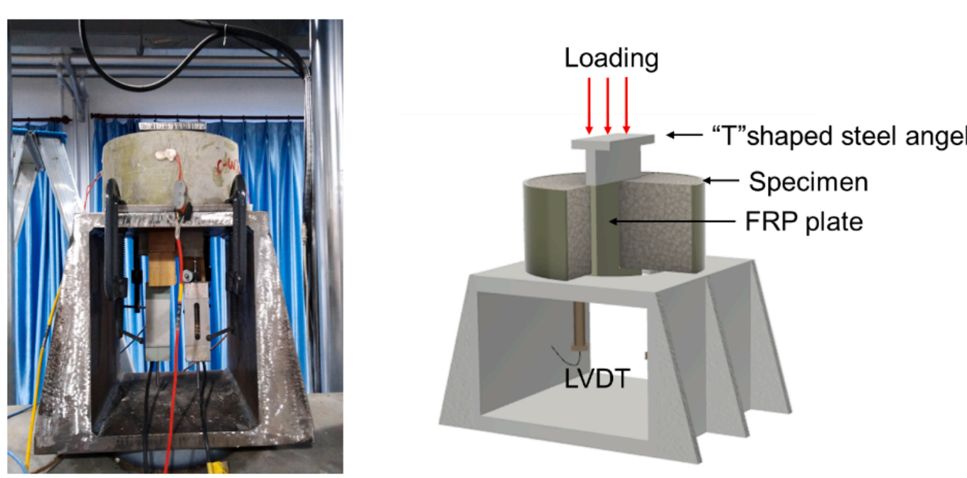

(b) Pushout tests

Fig. 3. Test setup of pullout and pushout tests.

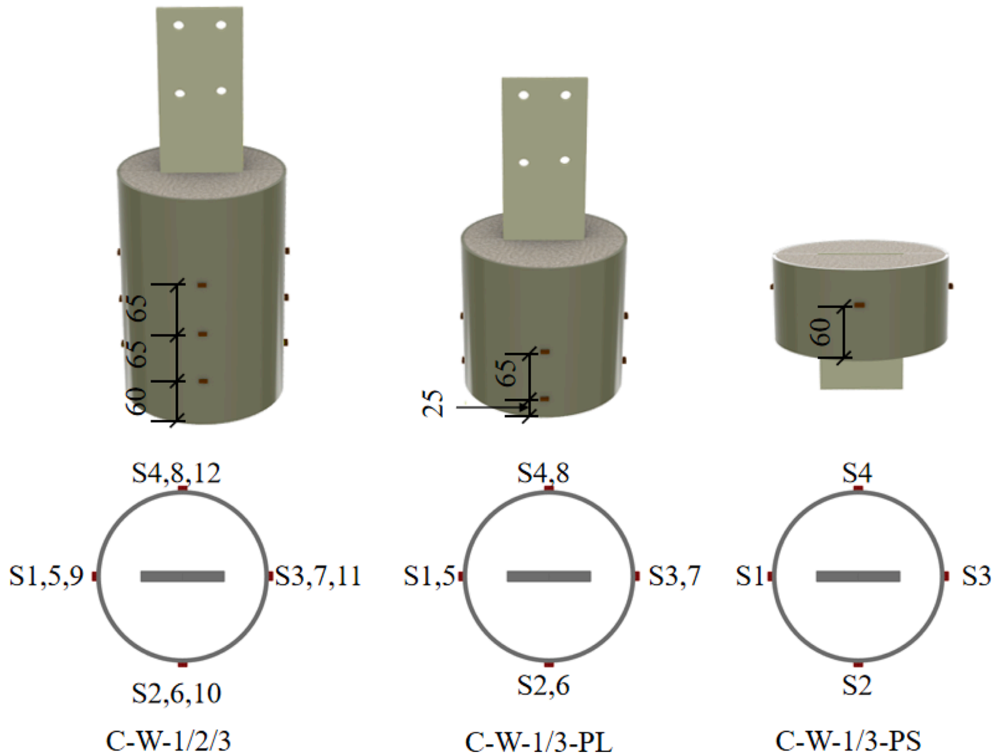

Fig. 4. Strain gauges for measuring hoop strain of FRP tube.

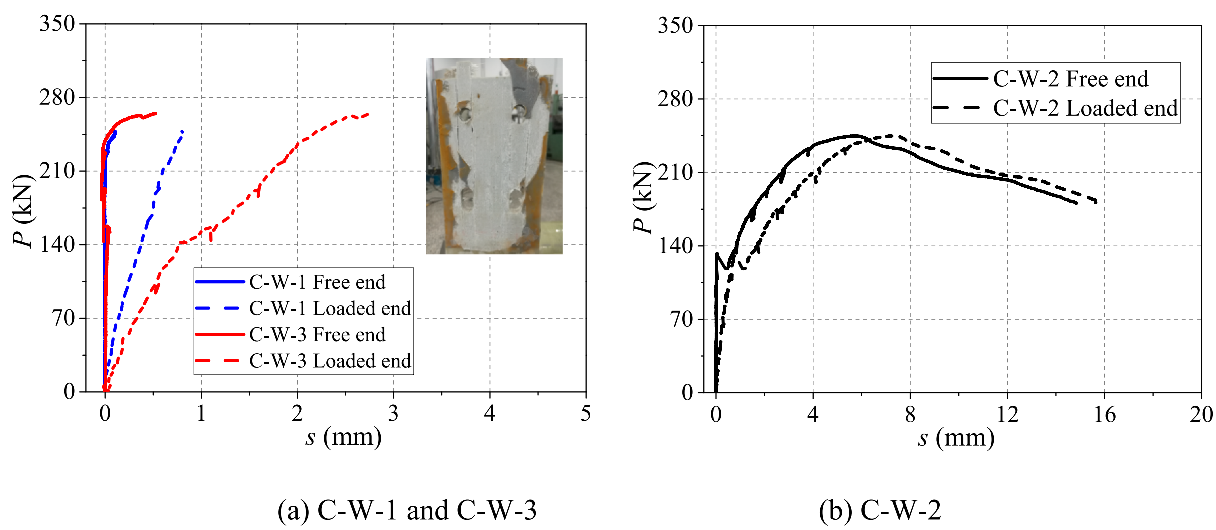

Fig. 5. Load-slip curves of long-bond length specimens.

2. Experimental program

2.1. Test specimen

Referring to the widely used central-pullout specimens for steel–concrete bond problems [42,43], a new pullout specimen for FRP-concrete interface is designed, as shown in Fig. 1. The specimen is consisted of a centrally embedded FRP plate, inner concrete and FRP tube. The FRP tube had an inner diameter of 200 mm, and a wall thickness of 4.5 mm. The FRP plate had a cross-section of 101.6 mm × 12.7 mm, and a length of 650 mm. For the bonded part of the plate, the plate surface was firstly roughened by sand papers, and then cleared by industrial alcohol. Finally, the plate was coated with a 1 mm-thick adhesive layer. Immediately after the adhesive coating, the FRP plate was centrally fixed in the FRP tube and the concrete was then cast.

Originally, the height of all the specimens was 300 mm with a bond length of 300 mm and a unbond length of 50 mm. In the unbond region, the FRP plate was isolated from the concrete via two foam blocks with a size of 101.6 mm × 20 mm × 50 mm. Due to the confining effect of FRP tube, the interfacial resistance of wet-bonding interface was so large that FRP material failure occurred at the clamping end. Full-range interfacial behavior was not obtained for two of the three specimens. Therefore, these two specimens were cut into two specimens after the first-round loading, one for pullout loading and the other one for pushout loading, as shown in Fig. 2. The pullout specimens had a bond length of 150 mm and an unbond length of 50 mm. The pushout specimens were 100 mm high with a bond length of 100 mm. Details about the tested specimens are shown in Table 1.

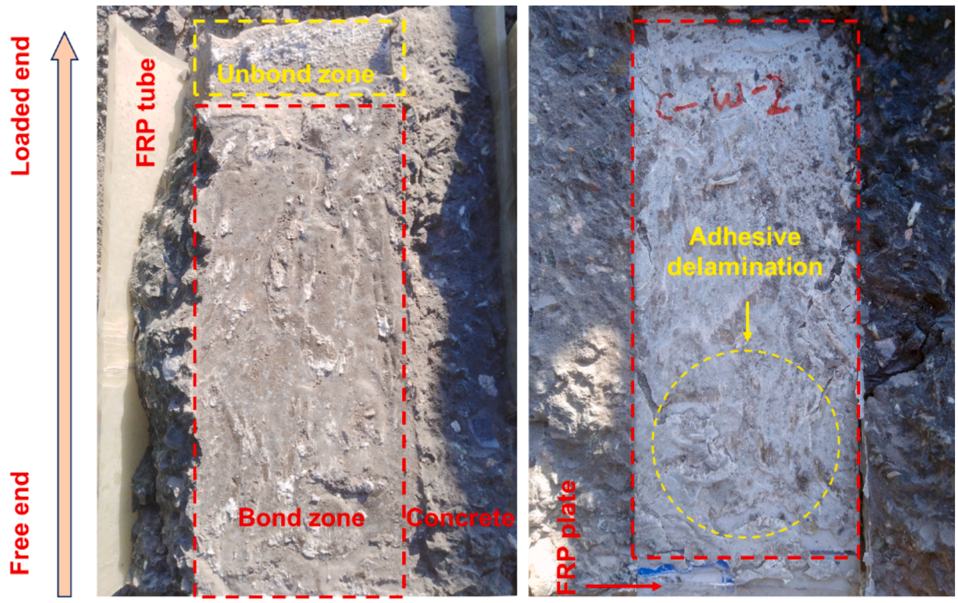

Fig. 6. The failure mode of specimen C-W-2.

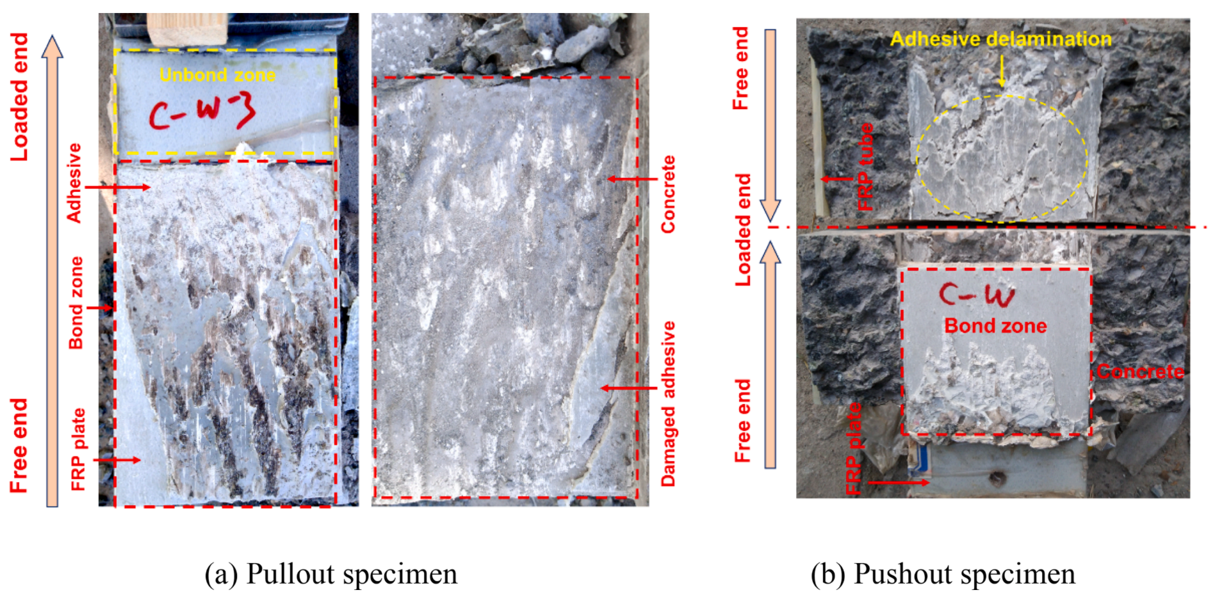

Fig. 7. The failure mode of short-bond length specimen.

2.2. Material properties

2.2.1. Concrete

C40 concrete was used for specimen fabrication, and its mixture proportion is shown in Table 2. Crushed limestone with a maximum grain size of 15 mm was used as the coarse aggregates. At the time of loading tests, the tested compressive strength of concrete on cubes (150 mm × 150 mm × 150 mm) and prisms (150 mm × 150 mm × 300 mm) were 45.7 MPa and 32.7 MPa, respectively.

2.2.2. FRP tube

The GFRP tube was made of E-glass fibers and epoxy resin through filament-winding technique. The fiber volume fraction was 75%, and the fiber orientation was ± 85° with respect to the longitudinal axis of the tubes. The mechanical properties of the tube were provided by the manufacture. The longitudinal and the hoop tensile strength were 41 MPa and 695 MPa, respectively. The hoop elastic modulus was 32.7 GPa.

2.2.3. FRP plate

The FRP plates were made of E-glass fibers and polyethylene resin matrix, and manufactured through a pultrusion technology. The mechanical properties of the pultruded plate were tested by the manufacturer, as listed in Table 3. Four holes with a diameter of 12 mm were created for bolt connection at the clamping end of the plate. To prevent potential FRP material failure at the clamping end, both sides of the plate were strengthened by two 6 mm-thick steel plates with a length of 180 mm. The steel plates were bonded to FRP plate through high strength adhesive.

2.2.4. Adhesive

The adhesive for wet-bonding interface was provided by Nanjing Hitech Composites Co Ltd. It’s a two-components modified construction epoxy adhesive, named as Lica-131A/B structural adhesive. The tested tensile strength and elastic modulus of the adhesive were 45 MPa and 7.2 GPa。.

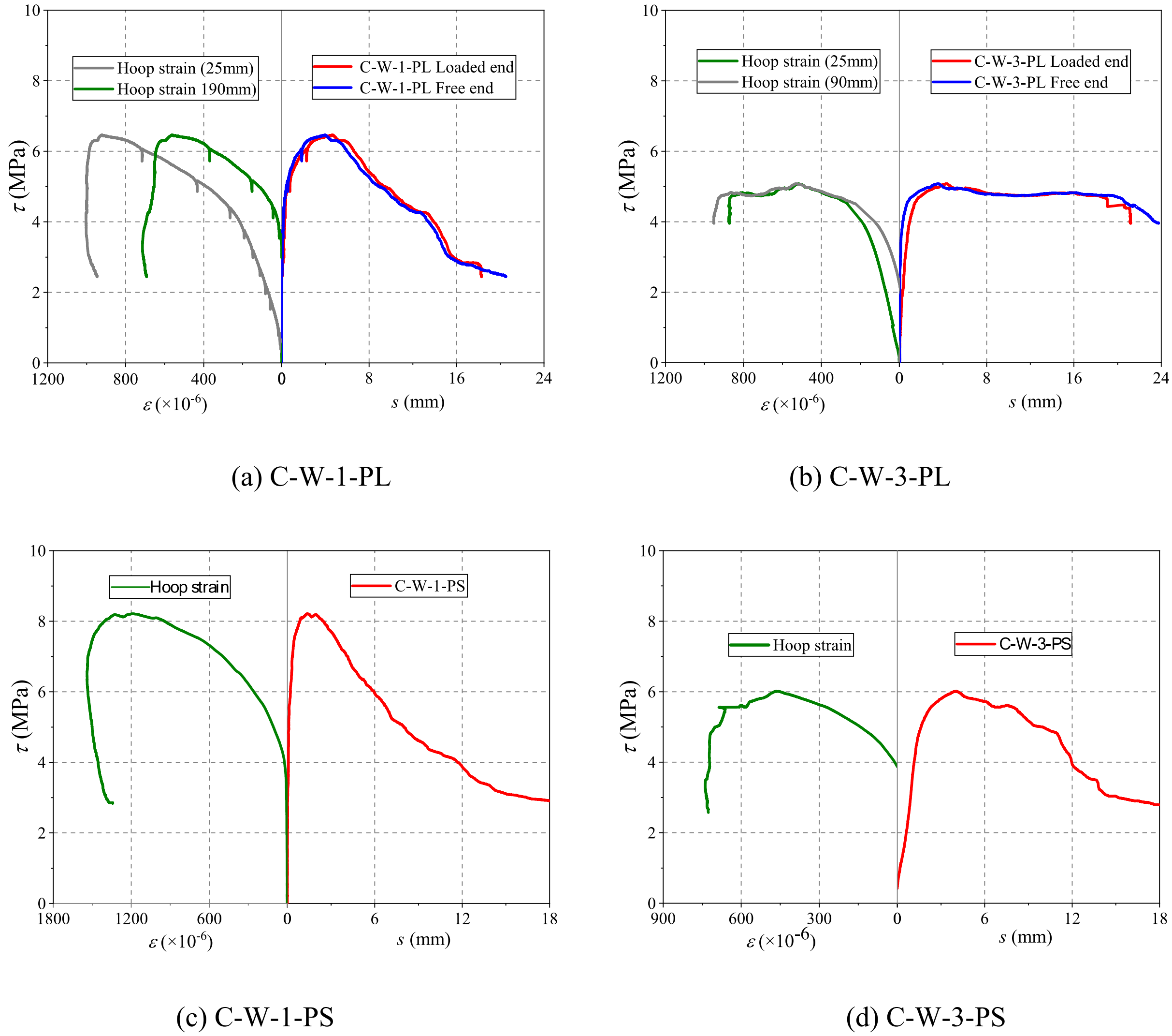

Fig. 8. Average bond stress-slip curves and development of hoop strain of FRP tube.

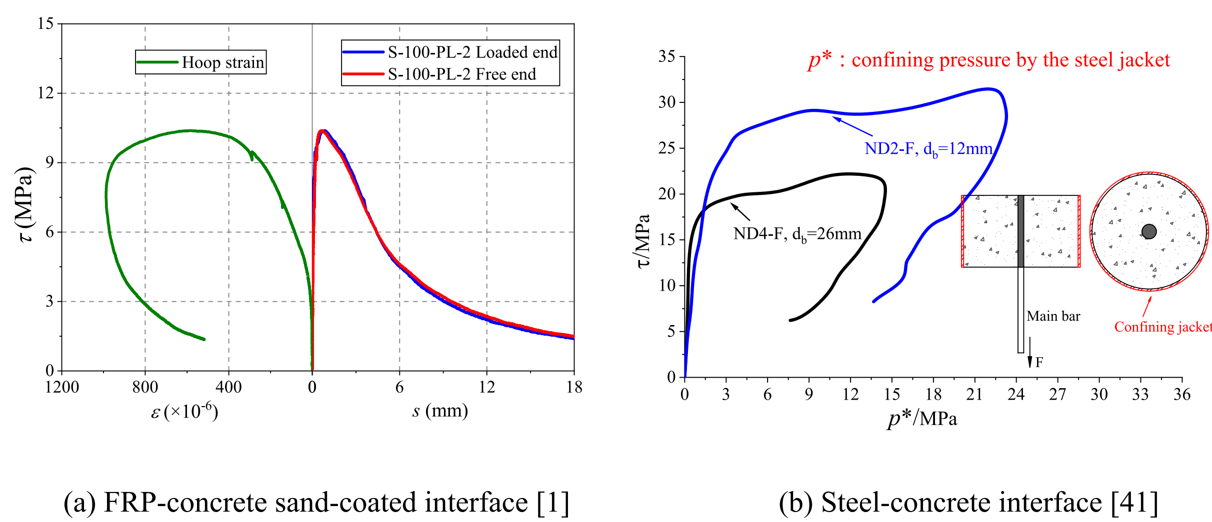

Fig. 9. Interfacial shear-dilatation phenomenon reported in the literature.

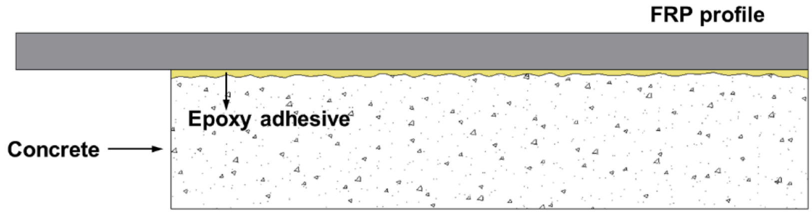

(a) Intact interface

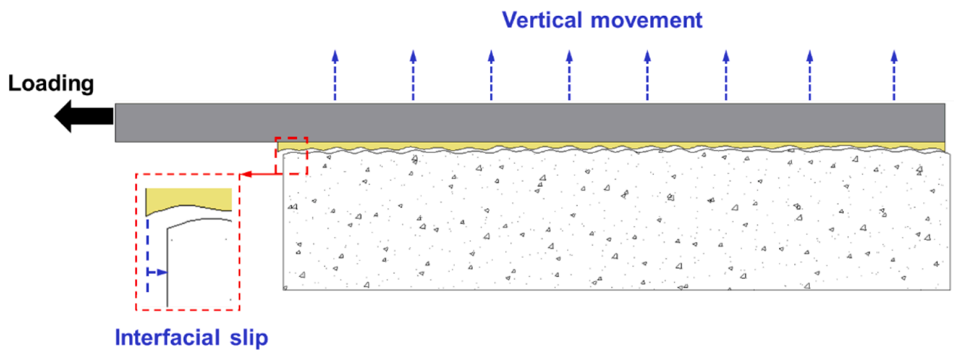

(b) Interface after initial debonding failure

Fig. 10. Schematic illustration of lateral movement induced by tangential sliding.

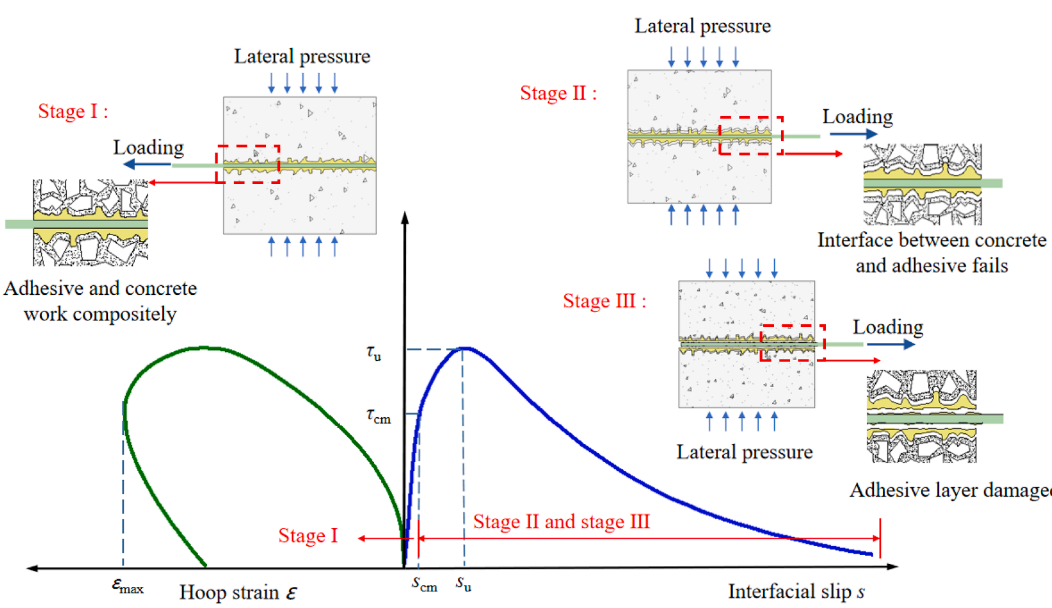

Fig. 11. Bond-slip mechanism of wet-bonding interface under lateral confinement.

2.3. Test setup and instrumentation

Fig. 3(a) shows the test setup for pullout loading. The specimen was constrained in a bespoke loading frame made of steel plate and screw rods. The lower part of the frame was connected to the universal testing machine through a spherical hinge, while the FRP plate of the specimen was connected to the university testing machine through three steel plates and a steel rod. The concrete of the specimen was in contact with the loading frame through a steel ring with an inner diameter of 65 mm and an outer diameter of 95 mm. The FRP plate was subjected to an upward load with a constant loading rate of 0.4 mm/min. To monitor the relative slips at the interface, two linear variable displacement transformers (LVDTs) were respectively installed at the free end and loaded end.

Fig. 3(b) shows the test setup for pushout loading. The specimen was seated on a bespoke reaction frame. The FRP plate was gradually pushed out from the concrete by a universal testing machine. A “T” shaped steel angle was used to transfer the load of universal testing machine to the FRP plate. Only two LVDTs were arranged at the free end of the specimen.

To monitor the development of hoop strain of the FRP tube, strain gauges were arranged at different heights. At each height, there were

Table 4
Bond stress-slip models for wet-bonding interface.

Literature	Expression	Key parameters
Wang et al. [32]	$\tau = 2BG_f\left[e^{(-Bs)} - e^{(-2Bs)}\right]$	$\tau_{max} = 0.5BG_f, s_{max} = \ln 2/B$, $G_f = 0.127(G_a/t_a)^{-0.812} f_c^{0.236}(E_f t_f)^{0.023}$, $B = 3.757(E_f t_f)^{0.108}(G_a/t_a)^{0.551}$.
where τ is the bond stress; s is the relative slip; τ_{max} and s_{max} are the ultimate bond stress and corresponding slip; G_f is the interfacial fracture energy; B is empirical parameter related with material properties; G_a and t_a are the shear modulus and thickness of adhesive layer; E_f and t_f are the elastic modulus and thickness of FRP plate.		
Zhang et al. [25]	$\tau = \tau_{max}(s/s_{max})^{0.5}(s \leqslant s_{max})$ $\tau = \tau_{max}e^{-\alpha(s/s_{max}-1)}(s > s_{max})$	$\tau_{max} = f_1\beta_w f_t, G_f = f_2\beta_w^2\sqrt{f_t}, s_{max} = f_3\beta_w f_t$, $\alpha = \frac{1}{\frac{G_f}{\tau_{max}s_{max}} - \frac{2}{3}}, \beta_w = \sqrt{\frac{2.25 - b_f/b_c}{1.25 + b_f/b_c}}$.
where τ is the bond stress; s is the relative slip; τ_{max} and s_{max} are the ultimate bond stress and corresponding slip; G_f is the interfacial fracture energy; α is coefficients in the proposed bond-slip models; β_w is the width ratio factor; f_1 is correction coefficient of the maximum shear stress; f_2 is the correction coefficient of the maximum fracture energy; f_3 is the correction coefficient of bond slip at the peak shear stress.		

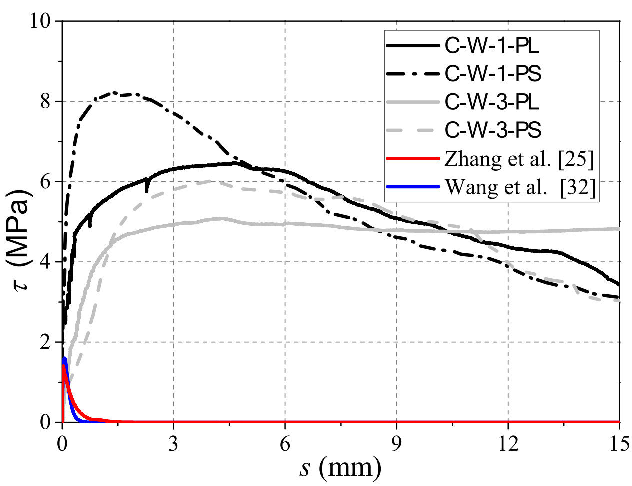

Fig. 12. Comparisons between tested curves and predicted curves by existing models.

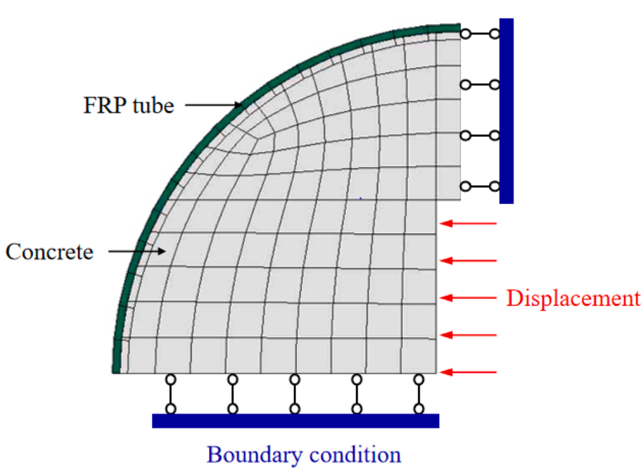

Fig. 13. FE model for the simulation of interfacial dilatation.

four strain gauges in the hoop direction, 90-degree apart. Fig. 4 shows the detailed positions of strain gauges.

All test data, including the strains, loads, and displacements, were automatically recorded by a computer-aided data acquisition system.

3. Experimental results

3.1. Long bond length specimens

When the pullout load was respectively 250 kN and 262 kN for specimen C-W-1 and C-W-3, the FRP plates failed in shear-out failure initiating from the bolt holes. Fig. 5 shows the tested load-slip curves.

The specimen C-W-2 failed at the concrete-adhesive interface, as shown in Fig. 6. Most of the adhesive layer had been detached from the concrete, and the bonding between adhesive and FRP plate was relatively good. Apparent scratch on the concrete and adhesive can be noticed. At the loaded end, the adhesive was in good bonding with FRP plate, while at the free end, part of the adhesive was delaminated from the plate. It's inferred that the failure first occurred at the concrete-adhesive interface (phenomenon at the loaded end). After that, significant friction took place between the adhesive and concrete, which further damaged the adhesive-FRP interface and resulted in the delamination of adhesive from the plate (phenomenon at the free end).

The load-slip curves of specimen C-W-2 can be divided into three stages: in the first stage, the load increased linearly until it reached 133 kN, then there was a sudden load drop. In this stage, the load began to show fluctuations at 72 kN. In the second stage, the load continued to increase until the peak load (245 kN). This stage was characterized with a reduced slope and apparent load fluctuations. It's believed that the load fluctuations are caused by the progressive failure of adhesive-concrete interface. In the third stage, i.e., after the peak, the load decreased gradually (ductile failure), which is very different with previous reports on the interfacial behavior of externally bonded FRP joint without any lateral confinements [44–46].

3.2. Short bond length specimens

All short bond length specimens, i.e., pullout and pushout specimens with a bond length of 150 mm or 100 mm, failed at the concrete-adhesive interface. As shown in Fig. 7, the failure mode of short-bond length specimens is quite similar to that of long-bond length specimens. Debonding failure firstly occurred at the adhesive-concrete interface and then at the adhesive-FRP interface due to significant friction between the adhesive layer and concrete. The evidence for this claim is the remarkable scratch on the adhesive and concrete. The location which experienced larger slip values had more severe adhesive damage. For instance, apparent adhesive delamination at the free-end of pullout specimens and loaded end of the pushout specimens can be observed.

In this study, it is assumed that the interfacial behavior of short-bond length specimens is close to a local bond behavior, and the bond stress is uniform along the bond length. The average bond stress can be calculated by the following equation,

$$\tau = \frac{P}{2Lb_f} \tag{1}$$

where P is the pushout or pullout load; L is the bond length; b_f is the width of FRP plate.

Fig. 8 shows the average bond stress-slip curves and corresponding hoop strain. As the FRP plate is gradually pulled out from the concrete, significant hoop strain is developed in FRP tube. This indicates an expansive interfacial behavior of wet-bonding interface, which has not been reported in previous studies. In the initial stage, the load increases rapidly, while the hoop strain is hardly developed. Once the load yields, the hoop strain starts to increase rapidly and finally shows a sign of

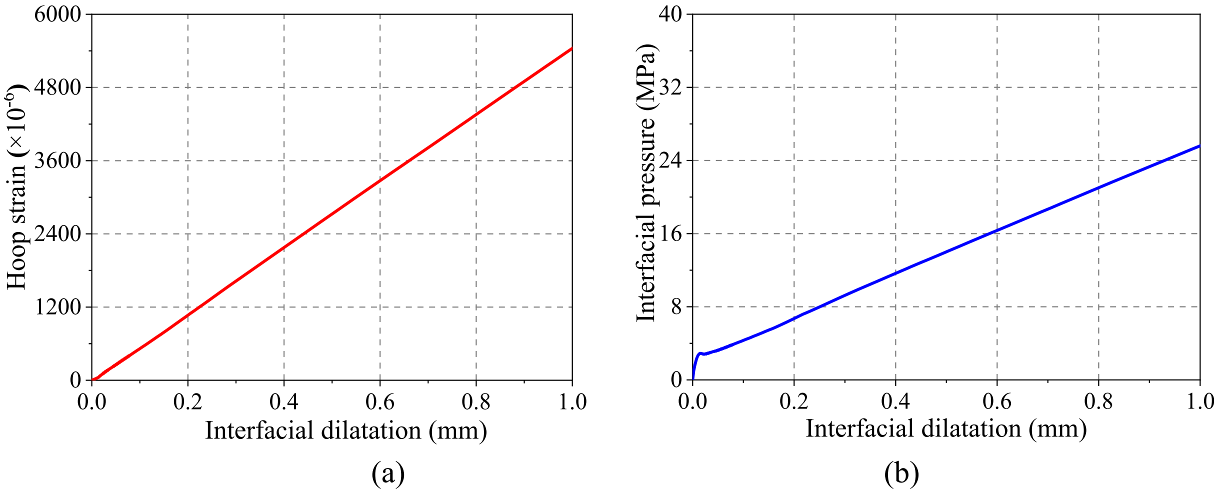

Fig. 14. Numerical results of the interfacial expansion behavior: (a) interfacial dilatation-hoop strain relationship; (b) interfacial dilatation-normal pressure relationship.

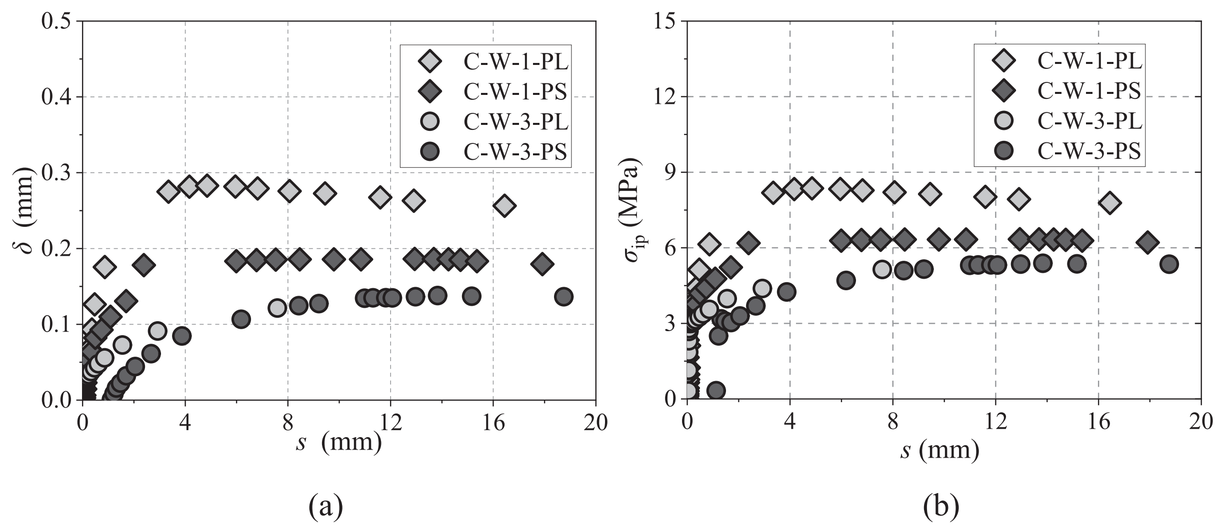

Fig. 15. Variation of interfacial dilatation (a) and pressure (b) with slip.

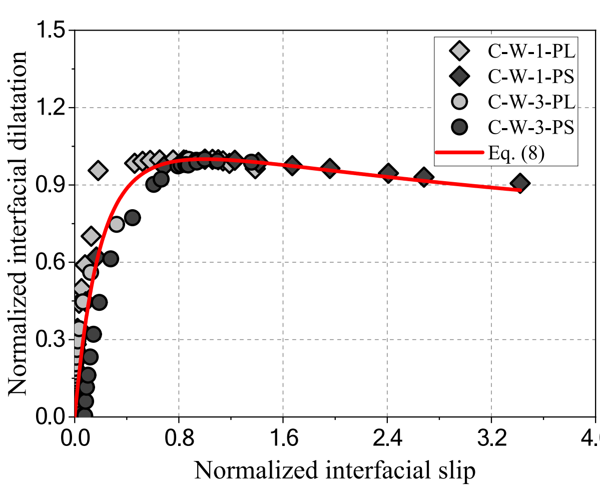

Fig. 16. Normalized interfacial dilatation-slip curve.

contraction. Similar phenomenon has been reported in other interfacial tests [3,47], see Fig. 9.

It's noteworthy that the tested curves of specimen C-W-3-PL show different shapes with other specimens. Compared with other specimens, specimen C-W-3-PL has a smaller peak bond stress and its post-peak bond stress shows no apparent reduction. The hoop strain shows no sign of contraction either. An explanation for this abnormal phenomenon is that the long-bond length specimen C-W-3 suffered serious interfacial damage in the first-round loading–unloading. According to the previous study by the authors [3], the force-transfer mechanism of wet-bonding interface is like that of sand-coated interface when lateral confinement is involved. Therefore, the tested bond stress-slip curves and the development of hoop strain of FRP tube should be similar. By comparing the curves in Fig. 8 and Fig. 9, it's considered that the specimen C-W-1-PL and C-W-1-PS are less affected by the first-round loading–unloading.

4. Discussions

4.1. Force-transfer mechanism

As summarized in the introduction, the bond strength of wet-bonding

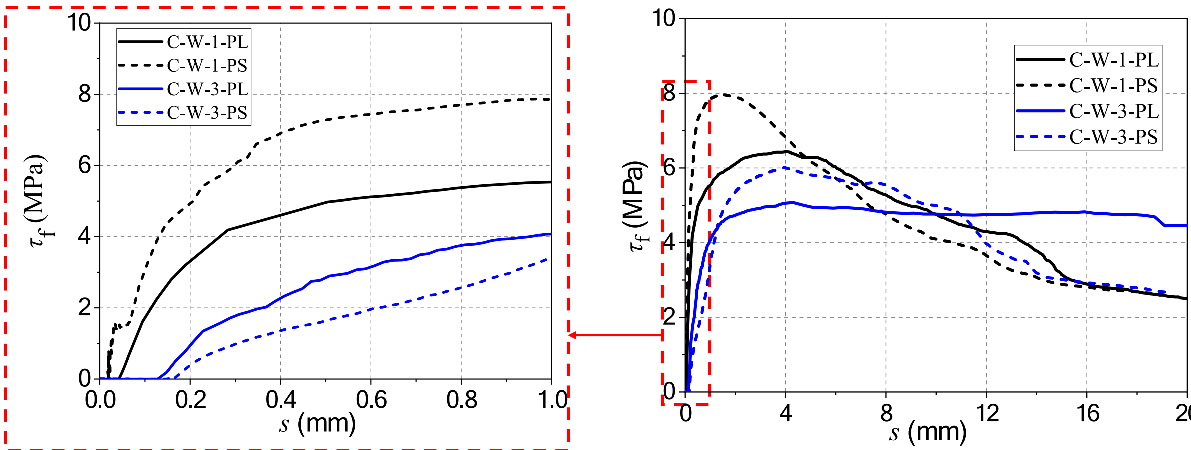

Fig. 17. Variation of friction components with slip.

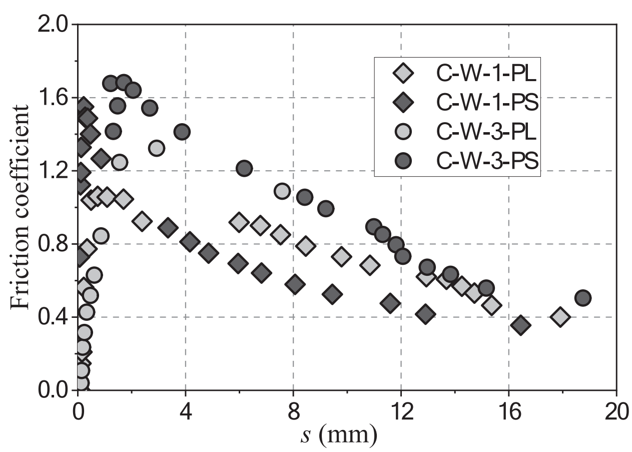

Fig. 18. Variation of friction coefficient with slip.

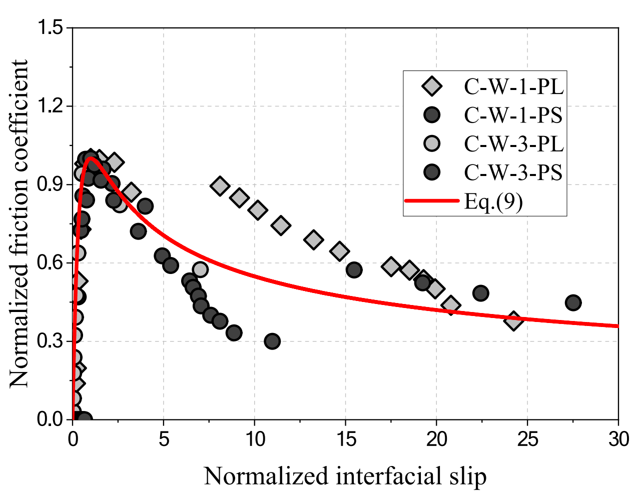

Fig. 19. Normalized friction coefficient-slip relationship.

interface is lower than that of dry-bonding interface due to the negative influence of moisture conditions in fresh concrete. The debonding failure occurs at the interface between concrete and adhesive layer. In this study, the same failure mode occurred initially. The formed fracture surfaces are rough due to the ingression of aggregates into the wet epoxy during concrete casting, see Fig. 10. When relative sliding between

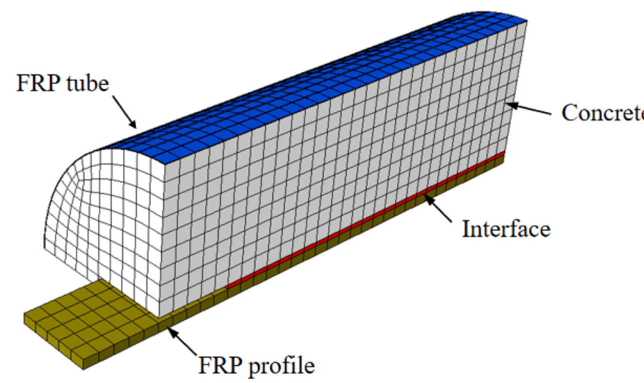

Fig. 20. 3D FE model of the long bond-length specimen.

fractured surfaces occurs, the mechanical interlock between *meso*-scale particles will induce vertical movement of interface. Consequently, the lateral confinement is activated, resulting in normal pressure and tangential friction at the interface. It should be noted that the alleged friction here is an overall description of friction and mechanical interlock at the interface. The significant friction behavior will further damage the adhesive layer and lead to adhesive debonding from the FRP plate.

Based on the above analysis, the interfacial behavior of wet-bonding interface can be divided into three stages, as shown in Fig. 11. (1) in stage I, the adhesive and concrete work compositely, and the interfacial slip comes from the shear deformation of concrete and adhesive layer. (2) in stage II, the interface between concrete and adhesive fails, and the further interactions between fractured surfaces result in interfacial dilatation, which activates the hoop confinement. Consequently, interfacial pressure and friction are developed at the interface. (3) in stage III, the interfacial friction increases and finally damages the adhesive layer, resulting in adhesive debonding from the plate and interfacial contraction.

4.2. Comparisons with existing bond stress-slip models

Numerous bond stress-slip models have been proposed for FRP-concrete interface in the literature. However, most of them are for dry-bonding interface, only two models proposed by Wang et al. [32] and Zhang et al. [25] are applicable for wet-bonding interface. These two models are based on bond models for dry-bonding interface and calibrated by test results of wet-bonding interface. Table 4 presents the expressions for the above two models.

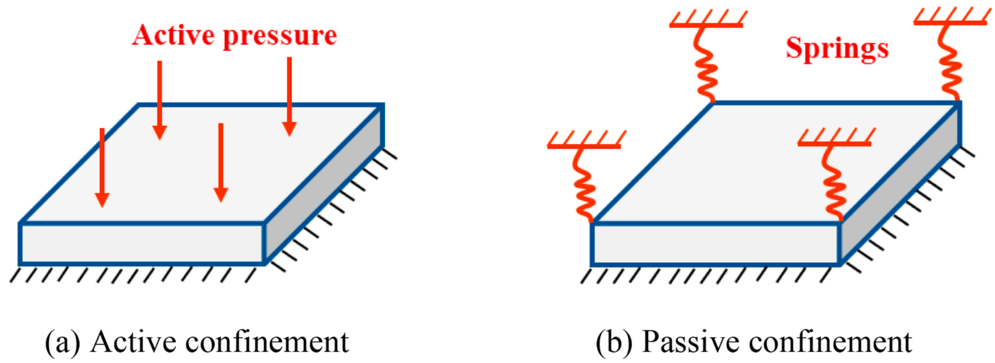

Fig. 21. Single element analysis of cohesive element.

In Fig. 12, the tested curves of short-bond length specimens are compared with the above two models. As can be seen, the predicted curves by the models are close, however, they are much lower than the tested curves. Initially, the ascending branches of predicted curves agree with tested curves, however, after the peak of predicted curves, considerable difference are exhibited. This reveals that current models cannot be adapted to conditions with lateral confinement. Before the generation of friction at the interface, previous models might still work, but after initial debonding, current models have limitations. The exact point where friction is generated is very difficult to determine, and as an approximation, it's considered that the friction is generated immediately after the initial interfacial debonding, i.e when $\tau = \tau_{cm}$.

5. Development of bond stress-slip model

5.1. Bond model for stage I

As illustrated above, in stage I, i.e., prior to the interfacial debonding, existing bond models for conditions without lateral confinement are applicable. In this paper, the bond model for wet-bonding interface proposed by Wang et al. [32] is adopted,

$$\tau_c(s) = 4\tau_{cm}\left[e^{(-Bs)} - e^{(-2Bs)}\right] \tag{2}$$

where τ_{cm} is the maximum bond stress in stage I; s_{cm} is the corresponding slip of τ_{cm}; B is an empirical parameter related with material properties. According to Wang et al. [32], $\tau_{cm} = 0.5BG_f$, $s_{cm} = \ln 2/B = 0.065$ mm, G_f is the interfacial fracture energy,

$$B = 3.757(E_f t_f)^{0.108}(G_a t_a)^{0.551} \tag{3}$$

$$G_f = 0.127(G_a/t_a)^{-0.812} f_c^{0.236}(E_f t_f)^{0.023} \tag{4}$$

where E_f and t_f are the elastic modulus and thickness of FRP plate; G_a is the shear modulus of adhesive layer; t_a is the thickness of adhesive layer.

5.2. Bond model for stage II and stage III

After the initial debonding failure, the lateral confinement is activated and the interfacial resistance comprises two components: remaining adhesion and generated friction. The adhesion reduces rapidly, and the friction is the main component. The interfacial resistance can be expressed by the following equation,

$$\tau(s) = \tau_c(s) + \tau_f(s) \tag{5}$$

where $\tau_f(s)$ is the friction component. The friction is determined by interfacial pressure and friction coefficient,

$$\tau_f(s) = \mu(s)\sigma_{ip}(s) \tag{6}$$

where $\mu(s)$ is the friction coefficient; $\sigma_{ip}(s)$ is the interfacial pressure. For passive confinement,

$$\sigma_{ip}(s) = K_{exp}(s)\delta \tag{7}$$

where $K_{exp}(s)$ is the lateral stiffness; δ is the interfacial dilatation.

5.2.1. Determination of pressure and expansion at the interface

As explained above, the interaction between fractured surfaces results in significant interfacial dilatation. To determine the interfacial pressure and expansion at the interface, the interfacial dilatation is simulated by FE models. A 3D FE model simulating the interfacial dilation was created by the commercial FE software Abaqus [48]. As shown in Fig. 13, only a quarter of the specimen was simulated and the FE model includes two parts, i.e. FRP tube and concrete. The concrete was modelled by solid elements C3D8R, and FRP tube was modelled by 4-node quadrilateral membrane elements M3D4R. The FRP tube was treated as a linear brittle material and its Poisson's ratio was set 0. For all the analyses, lateral displacements were uniformly imposed on the concrete surface within the bond zone. The nonlinear geometry NLGEOM option in Abaqus was turned on for all the analyses. The input compressive and tensile stress–strain data of concrete were determined according to the model by Teng et al. [49] and Hordijk. [50]. Concrete Damage Plasticity model provided by Abaqus was adopted. The dilation angle is 30, the eccentricity is 0.1, the ratio of biaxial compressive strength to axial compressive strength 1.16, and the ratio of biaxial compressive strength to triaxial compressive strength is 0.6667. The Youn's modulus and Poisson's ratio are 28418 MPa and 0.2, respectively.

After several trial parameter analyses, it was found that a mesh size of 10 mm can lead to reasonable numerical results. Moreover, the connection type between FRP tube and concrete has limited influence on the numerical results in the range of interest. Detailed discussions can be found in a previous paper by the authors [3]. Fig. 14 shows the interfacial dilatation-pressure curve and interfacial dilatation-hoop strain curve from numerical analyses. As can be seen, the interfacial pressure increases with the interfacial dilatation. In the first stage, the interfacial pressure increases with a gradually reducing stiffness, which is caused by concrete cracking. In the second stage, the interfacial pressure increases linearly with a lower stiffness than the first stage. It's considered that the lateral confinement in the second stage is mainly provided by FRP tube. Fig. 14(a) reveals that the hoop strain is in a linear relationship with the interfacial dilatation.

Based on the measured hoop strains of FRP tube and Fig. 14, the development of interfacial pressure and dilation of tested specimens can be determined, see Fig. 15. The interfacial pressure and dilatation all increase initially and then decrease gradually with the increase of slip. Similar phenomenon has been reported in the literature [3]. The initial increase of interfacial pressure and dilatation is due to the interlock between particles of the fractured interfaces. With the continued increase of interfacial slip, the particles were ground into fine particles and

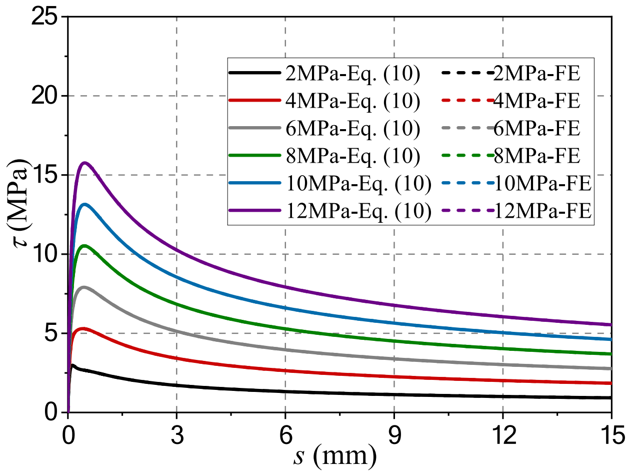

(a) Shear stress-slip curves for active confinement

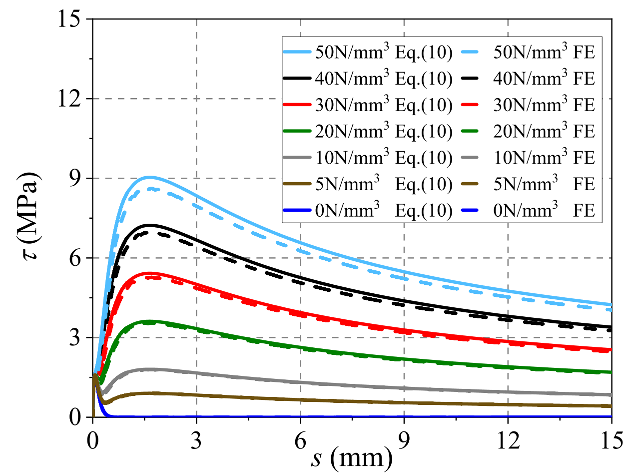

(b) Shear stress-slip curves for passive confinement

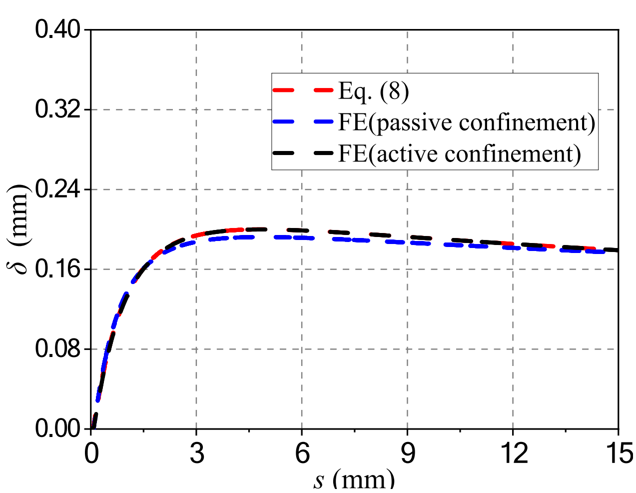

(c) Interfacial dilatation-slip curves

Fig. 22. Behavior of single cohesive element under different confinement conditions.

the bonding between FRP plate and adhesive layer was damaged, resulting in interfacial contraction and consequently smaller interfacial pressure.

To better show the variation of interfacial dilatation with slip, the curves in Fig. 15(a) are normalized, see Fig. 16. After normalization, the data scatter of the curves is much reduced, and a clear trend can be observed. According to the previous study by the authors, the following equation is used to describe the relationship between interfacial dilatation and slip,

$$\delta = 0 (0 \leqslant s \leqslant s_{cm}) \tag{8a}$$

$$\frac{\delta}{\delta_{max}} = \frac{s - s_{cm}}{s_{\delta_{max}} - s_{cm}} \frac{k_\delta}{k_\delta - 1 + \left(\frac{s - s_{cm}}{s_{\delta_{max}} - s_{cm}}\right)^{k_\delta}} (s_{cm} \leqslant s) \tag{8b}$$

where δ is the interfacial dilatation; δ_{max} and $s_{\delta max}$ are the maximum dilatation and corresponding slip; k_δ is an empirical parameter; s_{cm} is the slip value where the stage II initiates. Through data regression analysis, the following values are obtained, $\delta_{max} = 0.2$ mm, $s_{\delta max} = 4.85$ mm, $k_\delta = 1.23$. The fitted curve is in good agreement with the test data in Fig. 16.

5.2.2. *Friction coefficient*

As discussed above, the interfacial resistance is contributed by two components: chemical adhesion and friction. The chemical adhesion can be evaluated by Eq. (2). By subtracting the chemical adhesion from the tested curves, the friction component can be obtained, see Fig. 17. At the very beginning of the slip, no friction exists until the slip increases to a certain value. After the friction is developed, it firstly increases with the slip to the peak value and then decreases gradually.

According to Eq. (6), the variation of friction coefficient with slip can be obtained based on Fig. 15(b) and Fig. 17, see Fig. 18. The friction coefficient shows a similar trend with the interfacial dilatation. Similarly, Fig. 18 is normalized for reducing data scatter, see Fig. 19. The following equation is selected for describing the variation of friction coefficient with slip,

$$\frac{\mu(s)}{\mu_{max}} = \frac{s}{s_{\mu_{max}}} \frac{k_\mu}{k_\mu - 1 + \left(\frac{s}{s_{\mu_{max}}}\right)^{k_\mu}} \tag{9}$$

where μ_{max} and $s_{\mu max}$ are the maximum friction coefficient and corresponding slip, respectively. By fitting the data in Fig. 19, the values of parameters are determined, $\mu_{max} = 1.31$, $s_{\mu max} = 0.48$, k_μ=1.40.

5.3. *Full range bond model*

Substituting Eq. (2) and Eq. (6) into Eq. (5), the full range interfacial behavior of wet-bonding interface under lateral confinement can be obtained,

$$\tau(s) = 4\tau_{cm}\left[e^{(-Bs)} - e^{(-2Bs)}\right] + \mu(s)\sigma_{ip}(s) \tag{10}$$

where τ_{cm} is the maximum bond stress in stage I; B is a parameter related with material properties of FRP and adhesive, $B = 10.66$ according to Wang et al. [32]; G_f is the interfacial fracture energy, $G_f = 0.3$; $\mu(s)$ is the friction coefficient; $\sigma_{ip}(s)$ is the pressure at the interface.

5.4. *Verification of the proposed bond model*

A quarter model of the long bond length and short bond length specimens was respectively created using Abaqus. The interaction between FRP plate and concrete was simulated with cohesive elements (COH3D8) with a thickness of 1 mm. Other parameters of the FE model were the same with those in Section 5.2.1. Fig. 20 shows the FE model of long bond-length specimen.

The behavior of cohesive elements was governed by the proposed bond model, i.e, Eq. (2)-Eq. (10), where Eq. (8) and Eq. (10) determine

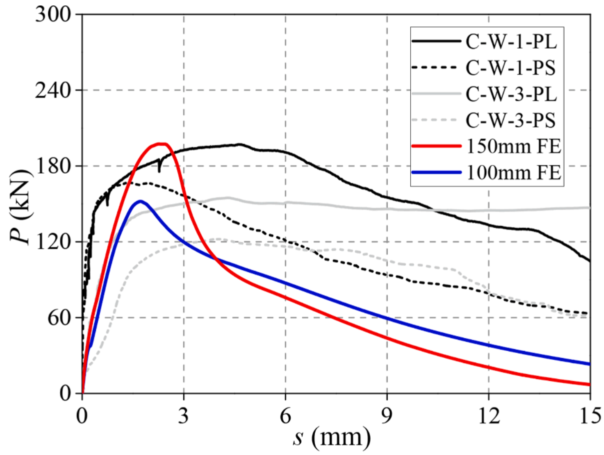

(a) Load-displacement relationship

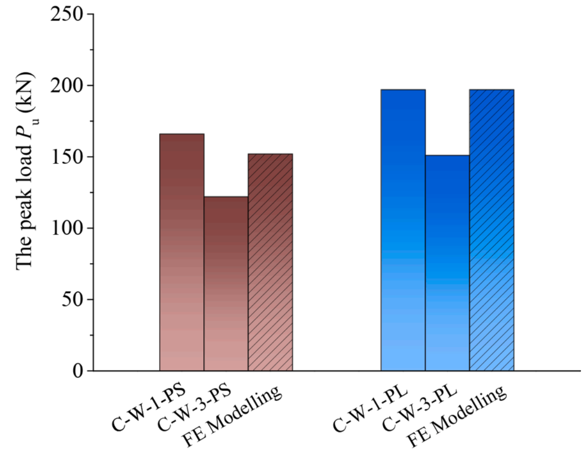

(b) The peak load

Fig. 23. Comparisons between numerical and teste results of short-bond length specimens.

the normal expansion and the shear stress at certain interfacial slip, respectively. To correlate the normal expansion with interfacial slip, a user-defined field variable (USDFLD) subroutine was programmed based on the cohesive elements. The interfacial expansion was activated through the "expansion" option in Abaqus, and the dependence of bond stress-slip relationship on interfacial pressure was achieved through the Solution-Dependent State Variable (SDV). In engineering structures, the lateral confinement includes two types: the passive confinement and the active confinement. The passive confinement is commonly seen in most scenarios, whereas the active confinement is less encountered. For instance, the lateral confinements of concrete by stirrups, FRP tube and steel tube, etc., all belongs to passive confinement. For concrete-filled steel tube column, spiral stirrups-confined concrete column, shape memory alloy (SMA) confined concrete column, when concrete is subjected to axial compression, the lateral confinement of concrete by yielded steel tube or yield stirrups or hoop prestress of SMA wires can be categorized as active confinement. To verify the effectiveness of the subroutine, the shear-dilatation behavior of a single cohesive element under both types of confinement was analyzed. Fig. 21(a) shows the single cohesive element under active confinement. The element is 10 mm in tangential direction and 1 mm in normal direction. Its lower surface is completely constrained, while the upper surface is subjected to normal pressure varying from 0 MPa ~ 12 MPa. Displacement loading is imposed on the upper surface. Fig. 22(a) shows the theoretical and numerical shear stress-relationship curves. The numerical curves are in complete agreement with theoretical curves. Fig. 21(b) shows the single element under passive confinement. The lower surface of the element is completely constrained, and the upper surface is connected to four springs with constant stiffness k_{spring} at the nodes. The lateral expansion stiffness $K_{\exp}$ varies from 0 N/mm^2 to 50 N/mm^2. The relationship between k_{spring} and $K_{\exp}$ is as follows,

$$k_{\text{spring}} = K_{\exp} l_{\text{coh}}^2 / 4 \tag{11}$$

where l_{coh} is the length of cohesive element, $l_{\text{coh}} = 10$ mm. Fig. 22(b) and Fig. 22(c) show the numerical interfacial shear stress and dilatation. For the passive confinement, the numerical shear stress and interfacial dilatation are slightly lower than theoretical values. This is because the cohesive element is assigned a limited value for the stiffness in the normal direction, which results in compression when normal pressure is developed. The reduction of interfacial expansion reduces normal pressure generated by passive confinement, and consequently reduces shear stress.

In Fig. 23, the numerical results are compared with the test results of short bond length specimens. In general, the predicted load-slip curves are slightly lower than the tested curves. The numerical peak load (P_u) of 100 mm-bond length and 150 mm-bond length specimens are 152 kN and 197 kN, respectively. The deviations between numerical and tested peak values are within 8%, see Fig. 23(b).

Comparisons of numerical and tested results of long bond length specimens are shown in Fig. 24. The ascending branch is well approached by FE modelling. The ultimate load which is not available by experimental tests is 295 kN by numerical modelling. The tensile strain of FRP plate and hoop strain of FRP tube at different locations are also well reproduced.

The loading–unloading history of long bond length specimens might have negative effects the test results of short bond length specimens. To have a general idea about the interfacial damage, the tensile stress of FRP plate, bond stress and interfacial slip of long bond length specimen at the load of 260 kN (the average of the tested peak load of C-W-1 and C-W-3) are extracted from the FE models, see Fig. 25. The interfacial slip and bond stress at the cutting plane are 0.6 mm and 4.2 MPa, respectively. This indicates that the first stage debonding has occurred within the bond zone from the free end to the cutting plane. Therefore, the first-round loading of long bond length specimens has caused damage to the pushout and pullout specimens. This may compromise the accuracy of the proposed model. Therefore, the proposed bond model should be further improved based on larger database in the future.

6. Parameter analysis based on the bond model

In order to have a more comprehensive understanding regarding the wet-bonding interface, a parameter analysis is conducted based on the FE model created in Section 5.4. The tensile stress of FRP plate, bond stress, interfacial slip and anchorage strength are respectively discussed, mainly focusing on the influence of lateral confinement on the interfacial behavior.

6.1. Distribution of tensile stress of FRP plate

Fig. 26 shows the tensile stress of FRP plate along the bond length. Before or after the peak load, the tensile stress of FRP plate at different locations increases with the load. The tensile stress decreases from the load end to the free end, showing an approximately linear distribution. This is much different with the phenomenon observed in FRP-concrete interface without lateral confinement. Fig. 27 shows the tested tensile strain of FRP plate along the bond length by Hunebum et al. [51] and

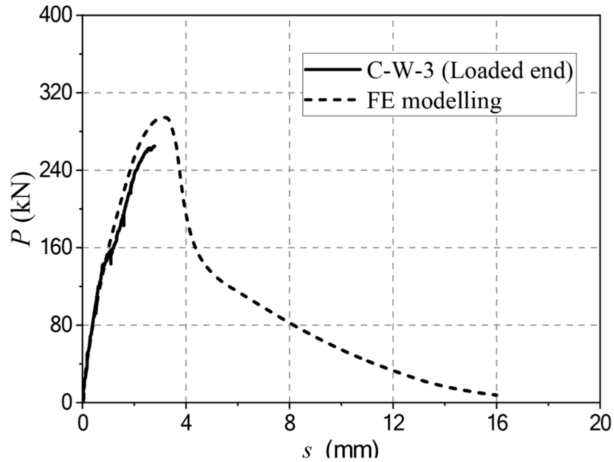

(a) Load-displacement relationship

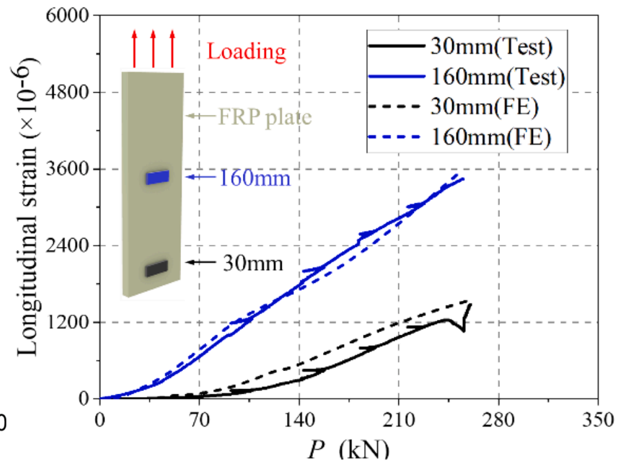

(b) Tensile strain of FRP plate

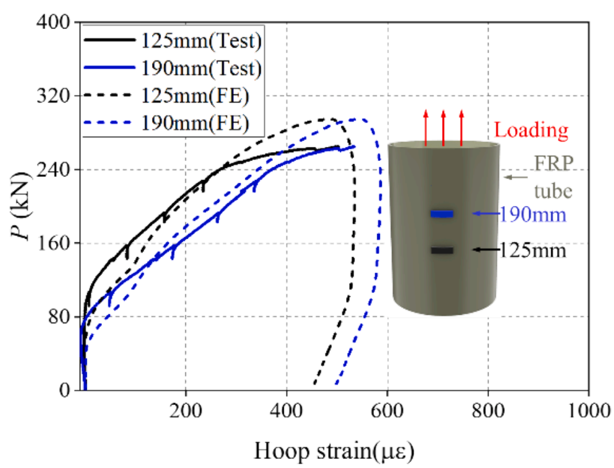

(c) Hoop strain of FRP tube

Fig. 24. Comparisons between numerical and test results of long bond-length specimens.

Chen et al. [52]. No lateral confinement is involved in their studies. A very different phenomenon can be observed, i.e, the tensile stress keeps constant in a certain region near the load end and this region extends with the increase of applied load. The fundamental reason for the difference is that the failure modes are different. Debonding failure firstly takes place near the load end. When no lateral confinement is involved, the bond zone with debonding failure can no longer transfer the load, and the tensile stress of FRP plate keeps constant. However, if the lateral confinement is present, friction between fractured surfaces will be developed immediately after debonding failure, and the tensile load of FRP plate will be gradually transferred to concrete through friction, resulting in continued decrease of tensile stress of FRP plate along the bond length.

6.2. Distribution of bond stress

Fig. 28 shows the bond stress along the bond length. At lower load levels, the bond stress is mainly developed in the bond zone near the load end with a single peak. When the load is increased, the bond stress is gradually developed near the free end, and a new peak is formed. The distribution of bond stress is saddle-shaped. Similar phenomenon has been observed in steel–concrete bond behavior [53,54]. According to previous studies, there is only one peak of bond stress along the bond length when no lateral confinement is involved. The only peak moves from the load end toward the free end with the increase of load-end slip. This reveals that the lateral confinement has greatly altered the distribution of bond stress along the bond length.

6.3. Distribution of interfacial slip

Fig. 29 shows the interfacial slip along the bond length. Before the peak load, the slip shows a nonlinear distribution along the bond length. The slip decreases from the load end to the free end, and the slip difference between the load end and the free end enlarges with increased load. After the peak, the slip tends to be uniform along the bond length.

6.4. Hoop strain of FRP tube

Fig. 30 shows the distribution of hoop strain of FRP tube. The hoop strain of FRP tube is non-uniform in both the hoop and vertical direction. It decreases from the load end to the free end. This phenomenon is more apparent at the I-I section. With the increase of applied load, the hoop

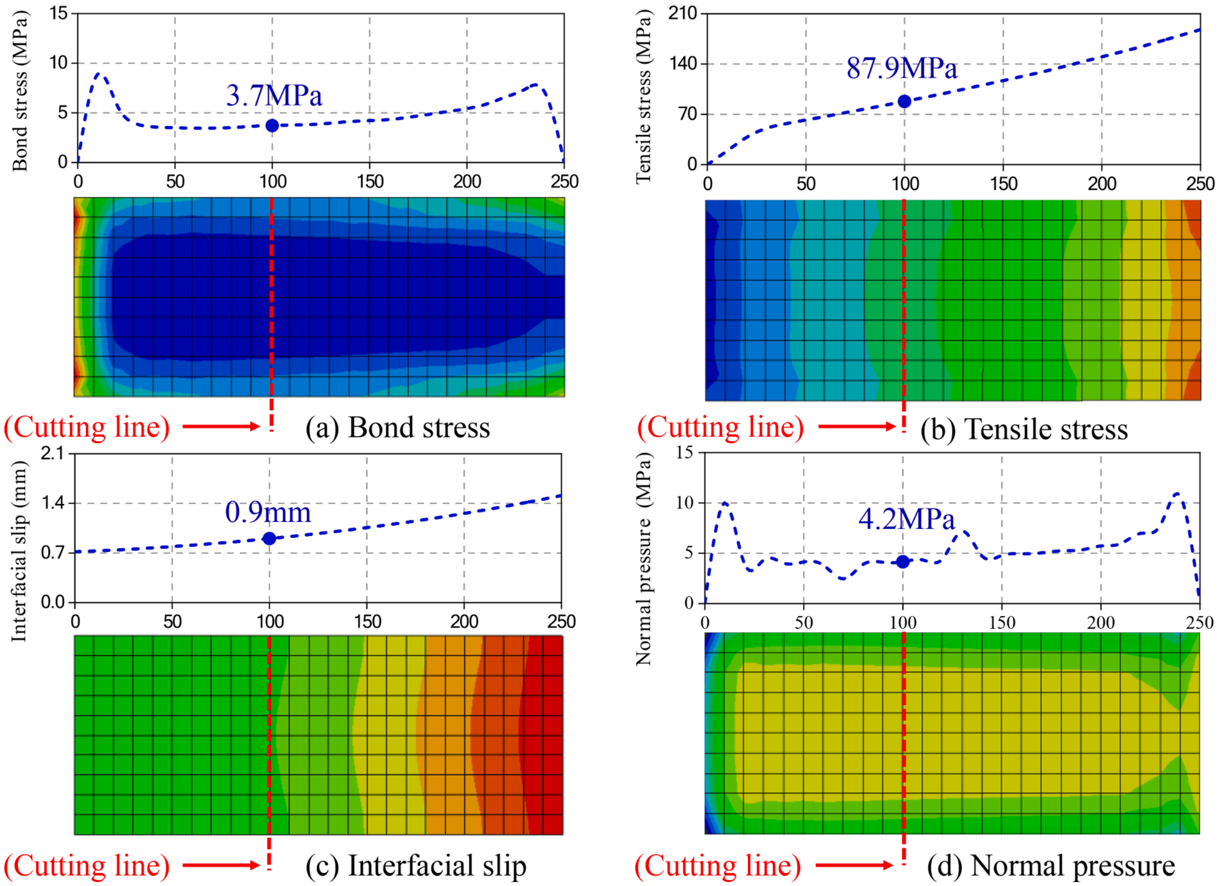

Fig. 25. State of the interface when plate failure occurs at the clamping end.

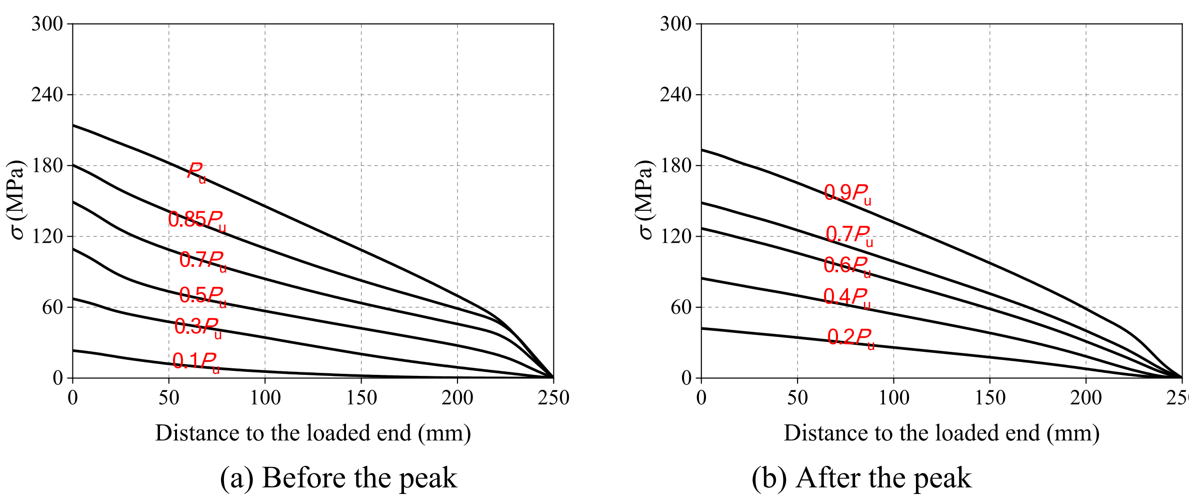

Fig. 26. Development of the tensile stress of FRP plate.

strain of FRP tube at the I-I section increases more rapidly compared with that at other sections. The concrete matrix at the I-I section also experiences more severe cracking, see Fig. 31.

6.5. Anchorage strength

To investigate the influence of bond length on the anchorage strength, FE models with different bond length were created. The geometrical size and material properties of FE models are the same with the tested specimens except for the bond length. The FE models simulating wet-bonding interface without lateral confinement adopt cohesive elements without expansion function, i.e. the normal pressure has no influence on the bond behavior. Fig. 32 shows the predicted anchorage strength of wet-bonding interface with or without lateral confinement.

For the conditions without lateral confinement, the anchorage strength increases with the bond length and reaches the peak when the bond length is around 300 mm. A further increase in bond length after 300 mm does not add anchorage strength. This is because there exists an effective bond length L_e, which governs the upper limit of anchorage

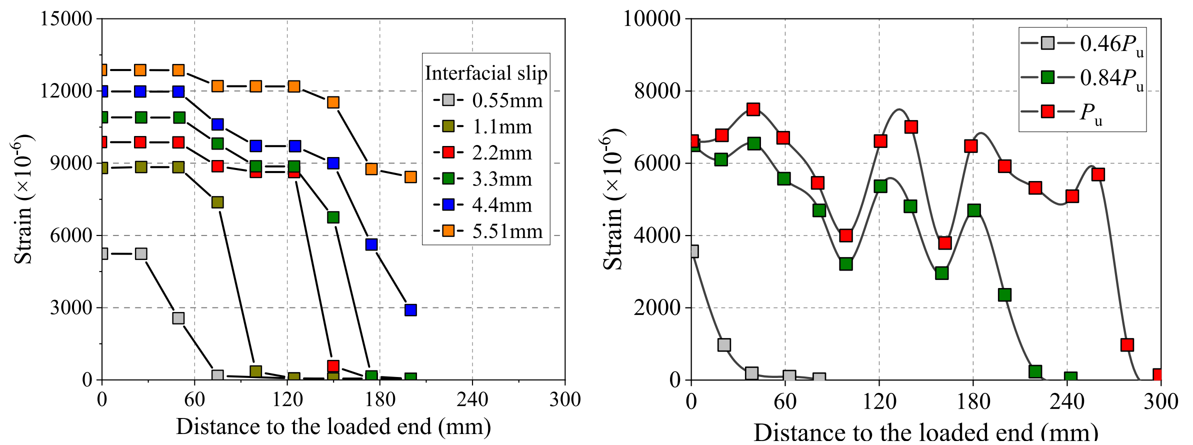

(a) Distribution of strain by Hunebum et al. [46] (b) Distribution of strain by Chen et al. [47]

Fig. 27. The distribution of FRP plate strain for conditions without confinement.

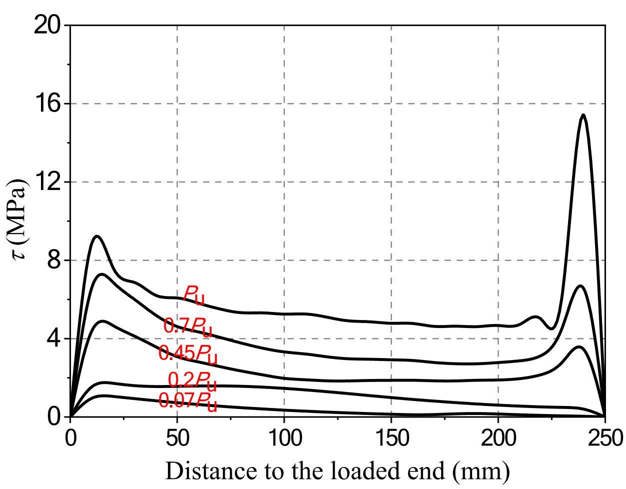

Fig. 28. The distribution of bond stress along the bond length.

strength. Many experimental and theoretical studies have confirmed that any increase in bond length cannot increase the anchorage strength when the bond length is larger than L_e [17,55,56]. Several empirical or theoretical equations for evaluating L_e can be found in the literature, and the following equation proposed by Lu et al. [57] is considered to agree well with various test results,

$$L_e = 1.33\frac{\sqrt{E_f t_f}}{f_t} \tag{12}$$

where, E_f and t_f are the tensile elastic modulus and thickness of FRP plate, respectively; f_t is the tensile strength of concrete. The calculated effective bond length according to Eq. (12) is 306 mm, which is very close with numerical value, see Fig. 32.

When the lateral confinement is introduced, the anchorage strength increases continuously with the bond length instead of plateauing at a certain bond length. Compared with the condition without lateral confinement, the anchorage strength with lateral confinement is considerably increased. For instance, for a bond length of 600 mm, the anchorage strength with lateral confinement is 7.2 times that without lateral confinement. It reveals that the FRP-concrete wet-bonding interface does not necessarily exist an effective bond length. It is dependent on the bond stress-slip relationship of the FRP-concrete

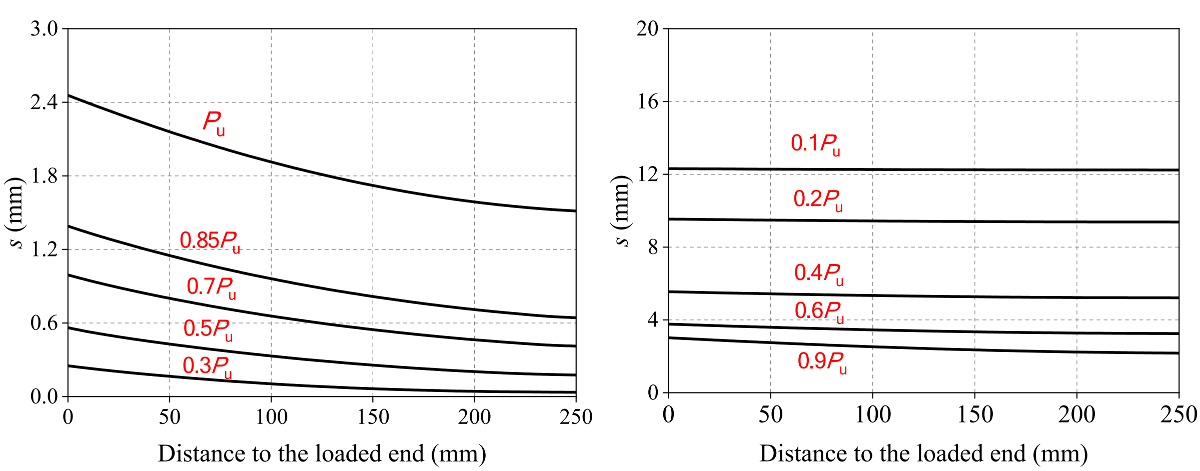

(a) Before the peak (b) After the peak

Fig. 29. The distribution of interfacial slip along the bond length.

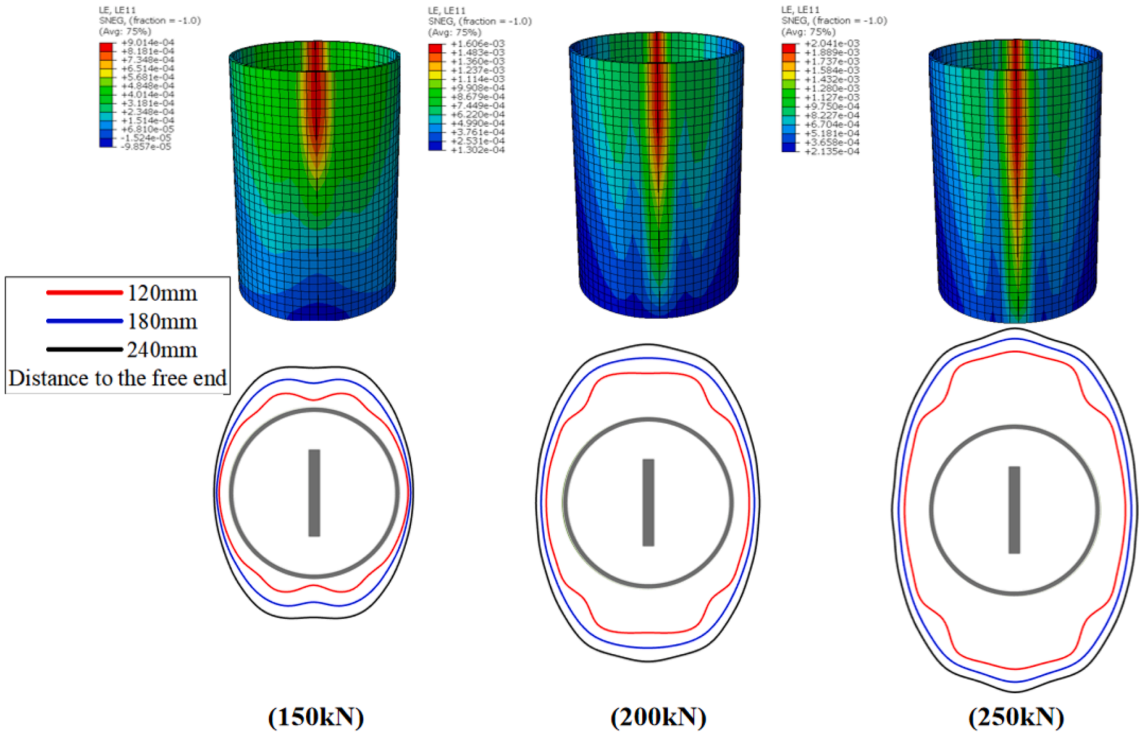

Fig. 30. Distribution of hoop strain of FRP tube.

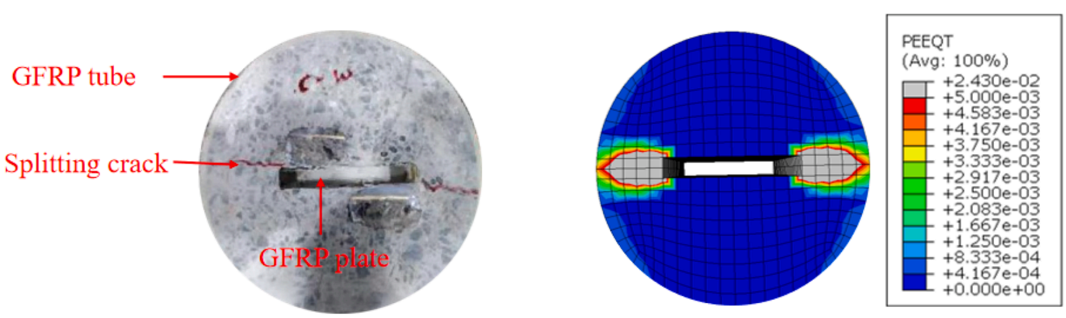

Fig. 31. Cracking pattern of concrete matrix of long bond-length specimen.

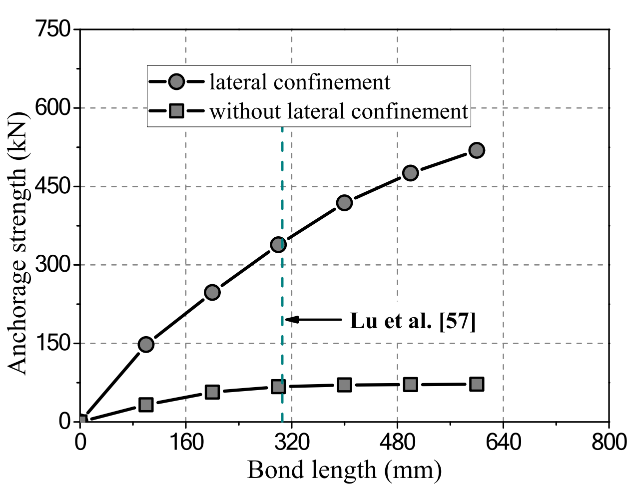

Fig. 32. Variation of anchorage strength with bond length.

interface.

7. Conclusion

This paper investigates the mechanical properties of wet-bonding interface under lateral confinement. Based on test results and numerical analysis, the following conclusions can be drawn:

(1) The progressive failure modes of long and short bond length specimens were similar, and their tested load-slip curves were ductile with gradually descending branches. For both types of specimens, significant hoop strains were developed in FRP tube when FRP plate was pulled out from concrete.
(2) For wet-bonding interface under lateral confinement, the debonding failure firstly occurred at the interface between concrete and adhesive layer, and then significant friction was developed between the fractured surfaces. The significant friction further damaged the adhesive layer, leaving the FRP plate without any concrete and adhesive attached.
(3) The bond-slip mechanism of wet-bonding interface under lateral confinement includes three stages. In the first stage, chemical bonding is dominant, while in the second and third stage which

are characterized by remarkable interfacial dilatation, the primary component of bond stress is the friction.

(4) Existing bond-slip models for wet-bonding interface cannot be adapted to conditions with lateral confinement due to the change in bond-slip mechanism. Based on existing bond models, a full stage bond-slip model for wet-bonding interface under different confinement conditions is developed. This model consists of several equations which respectively describe the development of friction coefficient, interfacial dilatation and shear stress with the interfacial slip.

(5) The proposed bond model can be used for the analysis of wet-bonding interface under active or passive confinement via FE software. The normal pressure at the interface can be automatically calculated by FE model, and bond-slip relationship will be dynamically updated. The bond model can provide reasonable predictions, but it needs further improvement based on a larger database.

(6) Parameter analysis based on the bond model indicates that the distribution of tensile stress of FRP plate, bond stress, interfacial slip, and the development of anchorage strength with bond length for wet-bonding interface are greatly altered by lateral confinement. Whether the FRP-concrete wet-bonding interface exists an effective bond length is dependent on the lateral confinement conditions of the interface.

CRediT authorship contribution statement

Hongwei Lin: Methodology, Funding acquisition. **Huixin Zeng:** Data curation, Formal analysis, Writing – original draft. **Peng Feng:** Conceptualization, Supervision. **Cheng Jiang:** Validation, Writing – review & editing. **Yuqing Zhang:** Validation.

Declaration of Competing Interest

The authors declare that they have no known competing financial interests or personal relationships that could have appeared to influence the work reported in this paper.

Data availability

Data will be made available on request.

Acknowledgements

This work was supported by the National Natural Science Foundation of China (No. 52108109 and U2106219), the Talent Fund of Beijing Jiaotong University (No. 2021RC232), the Open Research Fund by the Key Laboratory of Concrete and Pre-stressed Concrete Structure of Ministry of Education (CPCSME2018-02), and Australian Research Council (Grant No. DE210101662).

References

[1] Bank LC. Composites for construction: structural design with FRP materials. John Wiley & Sons; 2006.
[2] Feng P, Lu XZ, Ye LP. Application of fiber reinforced polymer in construction: experiment, theory and methodology. China Architecture & Building Press; 2011. In Chinese.
[3] Lin HW, Feng P, Yang JQ. Pressure-dependent bond stress-slip model for sand-coated FRP-concrete interface. Compos Struct 2021;263:113719.
[4] Yang JQ, Feng P. Analysis-oriented models for FRP-confined concrete: 3D interpretation and general methodology. Eng Struct 2020;216:110749.
[5] Wahan MY, Zhang Z, Meng X, Gao Y, Ji X. Mechanical behavior of GFRP-bamboo composite shear connections. Constr Build Mater 2022;331:127333.
[6] Zou XX, Lin HW, Feng P, Bao Y, Wang JQ. A review on FRP-concrete hybrid sections for bridge applications. Compos Struct 2021;262:113336.
[7] Nguyen H, Mutsuyoshi H, Zatar W. Push-out tests for shear connections between UHPFRC slabs and FRP girder. Compos Struct 2014;118:528–47.
[8] Zou XX, Feng P, Wang JQ. Perforated FRP ribs for shear connecting of FRP-concrete hybrid beams/decks. Compos Struct 2016;152:267–76.
[9] El-Hacha R, Chen D. Behaviour of hybrid FRP-UHPC beams subjected to static flexural loading. Compos Part B-Eng 2012;43(2):582–93.
[10] Garnevičius M, Gribniak V. Developing a hybrid FRP-concrete composite beam. Sci Rep 2022;12(1):1–9.
[11] Nguyen H, Zatar W, Mutsuyoshi H. Hybrid FRP-UHPFRC composite girders: Part 2–Analytical approach. Compos Struct 2015;125:653–71.
[12] Wang X, Su C, Deng W, Wu Z. Bond behavior between corrugated BFRP shell and concrete under monotonic and cyclic loads. Constr Build Mater 2019;210:596–606.
[13] Mo XD, Zeng WQ, Liao JJ, Zeng JJ. Flexural behavior of hybrid FRP-concrete-steel double-skin tubular beams with PBL shear connectors. Eng Struct 2022;254:113840.
[14] Fam AZ, Rizkalla SH. Behavior of axially loaded concrete-filled circular fiber-reinforced polymer tubes. Struct J 2001;98(3):280–329.
[15] Yu T, Wong YL, Teng JG, Dong SL, Lam ES. Flexural behavior of hybrid FRP-concrete-steel double-skin tubular members. J Compos Constr 2006;10(5):443–52.
[16] Hu L, Feng P, Lin HW, Yang JQ, Qiang HL. Seismic performance of composite shear walls with embedded FCCCs in boundary elements. Compos Struct 2021;257:113126.
[17] Chen JF, Teng JG. Anchorage strength models for FRP and steel plates bonded to concrete. J Struct Eng 2001;127(7):784–91.
[18] Hulatt JA, Hollaway LC, Thorne A. A novel advanced polymer composite/concrete structural element. Struct Build 2004;157:9–17.
[19] Wu ZS, Yang CQ, Iwashita K, Mishima H. Development of damage-controlled latter cast FRP–RC hybrid girders. Compos Part B: Eng 2011;42:1770–2177.
[20] Canning L, Hollaway L, Thorne AM. An investigation of the composite action of an FRP/concrete prismatic beam. Constr Build Mater 1999;13:417–26.
[21] Honickman H, Nelson M, Fam A. Investigation into the bond of Glass Fiber-Reinforced Polymer Stay-in-Place structural forms to concrete for decking applications. Transp Res Rec 2009;2131:134–44.
[22] Shao Y, Wu ZS, Bian J. Wet-bonding between FRP laminates and cast-in-place concrete. Int. Symposium on Bond Behaviour of FRP in Structures, IIFC, Hong Kong; 2005.
[23] Li L, Shao YX, Wu ZS. Durability of wet bond of hybrid laminates to cast-in-place concrete. J Compos Constr 2010;14(2):209–16.
[24] Zhang L, Wang WW, Harries KA, Tian J. Bonding behavior of wet-bonded GFRP-concrete interface. J Compos Constr 2015;19(6):4015001.
[25] Zhang P, Wu G, Zhu H, Meng SP, Wu ZS. Mechanical performance of the wet-bond interface between FRP plates and cast-in-place concrete. J Compos Constr 2014;18(6):4014016.
[26] Zhang P, Zhu H, Wu G, Meng SP, Wu ZS. Shear capacity comparison of four different composite interfaces between FRP plates and concrete substrate. J Compos Constr 2016;20(4):4016006.
[27] Zhang P, Gao DY, Zhu H. Numerical simulation and experimental study on the performance of wet-bonding interface between FRP plate and concrete. China Civ Eng J 2013;46(2):108–14. in Chinese.
[28] Dai JG, Ueda T, Sato Y. Development of the nonlinear bond stress-slip model of fiber reinforced plastics sheet-concrete interfaces with a simple method. J Compos Constr 2005;9(1):52–62.
[29] Lu XZ, Teng JG, Ye LP, Jiang JJ. Bond–slip models for FRP sheets/plates bonded to concrete. Eng Struct 2005;27(6):920–37.
[30] Lu XZ, Jiang JJ, Teng JG, Ye LP. Finite element simulation of debonding in FRP-to-concrete bonded joints. Constr Build Mater 2006;20(6):412–24.
[31] Lu XZ, Ye LP, Teng JG, Jiang JJ. Meso-scale finite element model for FRP sheets/plates bonded to concrete. Eng Struct 2005;27(4):564–75.
[32] Wang WW, Huang H, Zhao F. Experimental study on bonding behavior of GFRP plate and concrete interface based on wet bonding technique. China Civ Eng J 2015;48(3):52–60. in Chinese.
[33] Giv AN, Fu QN, Yan LB, Kasal B. Interfacial bond behavior of adhesively-bonded timber/cast in situ concrete (wet bond process). Acta Polytech CTU Proc 2022;33:398–403.
[34] Giv AN, Fu QN, Yan LB, Kasal B. Interfacial bond strength of epoxy and PUR adhesively bonded timber-concrete composite joints manufactured in dry and wet processes. Constr Build Mater 2021;311:125356.
[35] Hadi MN, Yuan JS. Experimental investigation of composite beams reinforced with GFRP I-beam and steel bars. Constr Build Mater 2017;144:462–74.
[36] Li GC, Sun X, Yang ZJ, Fang C, Chen BW, Ge HB, et al. Structural performance of concrete-filled square steel tubular columns encased with I-shaped CFRP under eccentric compression. Eng Struct 2021;248:113254.
[37] Feng P, Li ZY, Wang J, Liu TQ. Novel joint for pultruded FRP beams and concrete-filled FRP columns: Conceptual and experimental investigations. Compos Struct 2022;287:115339.
[38] Biscaia HC, Chastre C, Silva MA. Bond-slip model for FRP-to-concrete bonded joints under external compression. Compos Part B-Eng 2015;80:246–59.
[39] Lee J, Lopez MM. Characterization of FRP Uwrap anchors for externally bonded FRP-reinforced concrete elements: An experimental study. J Compos Constr 2016;20(4):4016012.
[40] Lee J, Lopez MM. Frictional bond-slip model for the concrete-FRP interface under the FRP U-wrap region. Constr Build Mater 2019;194:226–37.
[41] Zhou YW, Wang XW, Sui LL, Xing F, Huang ZY, Chen C, et al. Effect of mechanical fastening pressure on the bond behaviors of hybrid-bonded FRP to concrete interface. Compos Struct 2018;204:731–44.
[42] Qian SZ, Li VC. Influence of concrete material ductility on headed anchor pullout performance. ACI Mater J 2009;106(1):72–81.
[43] Lin HW, Zhao YX, Feng P, Ye HL, Ozbolt J, Jiang C, et al. State-of-the-art review on the bond properties of corroded reinforcing steel bar. Constr Build Mater 2019;213:216–33.

[44] Yuan H, Teng JG, Seracino R, Wu ZS, Yao J. Full-range behavior of FRP-to-concrete bonded joints. Eng Struct 2004;26(5):553–65.
[45] Wu YF, Xu XS, Sun JB, Jiang C. Analytical solution for the bond strength of externally bonded reinforcement. Compos Struct 2012;94(11):3232–329.
[46] Wu YF, Jiang C. Quantification of bond-slip relationship for externally bonded FRP-to-concrete joints. J Compos Constr 2013;17(5):673–86.
[47] Lin HW, Zhao YX, Ozbolt J, Feng P, Jiang C, Eligehausen R. Analytical model for the bond stress-slip relationship of deformed bars in normal strength concrete. Constr Build Mater 2019;198:570–86.
[48] Abaqus. ABAQUS Analysis User's Manual. Version 2013;6:13.
[49] Teng JG, Huang YL, Lam L, Ye LP. Theoretical model for fiber-reinforced polymer-confined concrete. J Compos Constr 2007;11(2):201–10.
[50] Hordijk PA. Local approach to fatigue of concrete. PhD. Thesis. Netherland: Delft University; 1991.
[51] Ko H, Sato Y. Bond stress-slip relationship between FRP sheet and concrete under cyclic load. J Compos Constr 2007;11(4):419–26.
[52] Chen C, Li X, Zhao DB, Huang ZY, Sui LL, Xing F, et al. Mechanism of surface preparation on FRP-Concrete bond performance: a quantitative study. Compos Part B-Eng 2019;163:193–206.
[53] Zhao YX, Lin HW, Wu K, Jin WL. Bond behaviour of normal/recycled concrete and corroded steel bars. Constr Build Mater 2013;48:348–59.
[54] Zhang WP. Corrosion damage prediction and durability evaluation of steel reinforcement in concrete structures. PhD. Thesis, Tongji University, Shanghai; 1999 [in Chinese].
[55] Nakaba K, Kanakubo T, Furuta T, Yoshizawa H. Bond behavior between fiber-reinforced polymer laminates and concrete. ACI Struct J 2001;98(3):359–67.
[56] Mostofinejad D, Arefian B. Generic assessment of effective bond length of FRP-concrete joint based on the initiation of debonding: Experimental and analytical investigation. Compos Struct 2021;277:114625.
[57] Lu XZ. Studies on FRP-concrete interface. PhD. Thesis, Tsinghua university, Beijing; 2004 [in Chinese].